Advanced Review

# First-principles modeling of molecular crystals: structures and stabilities, temperature and pressure

Johannes Hoja,[1,2] Anthony M. Reilly[3] and Alexandre Tkatchenko[1,2]*

The understanding of the structure, stability, and response properties of molecular crystals at finite temperature and pressure is crucial for the field of crystal engineering and their application. For a long time, the field of crystal-structure prediction and modeling of molecular crystals has been dominated by classical mechanistic force-field methods. However, due to increasing computational power and the development of more sophisticated quantum-mechanical approximations, first-principles approaches based on density functional theory can now be applied to practically relevant molecular crystals. The broad transferability of first-principles methods is especially imperative for polymorphic molecular crystals. This review highlights the current status of modeling molecular crystals from first principles. We give an overview of current state-of-the-art approaches and discuss in detail the main challenges and necessary approximations. So far, the main focus in this field has been on calculating stabilities and structures without considering thermal contributions. We discuss techniques that allow one to include thermal effects at a first-principles level in the harmonic or quasi-harmonic approximation, and that are already applicable to realistic systems, or will be in the near future. Furthermore, this review also discusses how to calculate vibrational and elastic properties. Finally, we present a perspective on future uses of first-principles calculations for modeling molecular crystals and summarize the many remaining challenges in this field. 

How to cite this article:
*WIREs Comput Mol Sci* 2017, 7:e1294. doi: 10.1002/wcms.1294

## INTRODUCTION

Molecular crystals are versatile materials that find applications as pharmaceuticals, explosives, organic semiconductors, in solid-state reactions, and plastic materials.[1–8] Molecular crystals are solids composed of well-defined molecular moieties that are held together by noncovalent forces (intermolecular interactions). These interactions between molecules are typically weaker than intramolecular covalent bonds or bonds in hard solid materials. However, an understanding of intermolecular interactions is crucial for the fast-growing field of crystal engineering, where the main goal is to design and ultimately synthesize new crystalline materials with a predefined arrangement of molecules that exhibit certain properties and functionalities.[9,10] This involves specific self-organization and self-recognition of molecules, which is governed by intermolecular interactions. In this context, recognition events are often discussed in terms of specific intermolecular interactions such as hydrogen bonds, $\pi$-$\pi$ stacking, C–H$\cdots\pi$ interactions, halogen bonds, dipole–dipole

*Correspondence to: alexandre.tkatchenko@uni.lu

[1]Fritz-Haber-Institut der Max-Planck-Gesellschaft, Berlin, Germany

[2]Physics and Materials Science Research Unit, University of Luxembourg, Luxembourg City, Luxembourg

[3]The Cambridge Crystallographic Data Centre, Cambridge, UK

Conflict of interest: The authors have declared no conflicts of interest for this article.

  

interactions, and van der Waals (vdW) interactions.[10] In order to model all these interactions correctly and achieve predictive power, classical force fields are often insufficient and the use of first-principles methods is required.

For small molecular dimers, the intermolecular interaction energy can be calculated rather accurately with quantum-chemical coupled cluster techniques[11] or the quantum Monte Carlo (QMC) method.[12] Such explicitly correlated approaches have been used as benchmarks for several datasets of noncovalent interactions.[13–15] However, these methods are only applicable to relatively small systems due to their rather high computational cost. Therefore, in recent years density functional theory (DFT) has emerged as the first-principles method of choice for larger systems, especially with the continuing development of improved density functional approximations (DFA) and the incorporation of the long-range vdW energy via several models for dispersion interactions.[16–22]

However, the quality of interaction energies is not always optimal with vdW-inclusive DFA approaches. For example, the accuracy of DFA+vdW for strong hydrogen bonds and charge transfer can be sometimes inadequate.[23] For periodic molecular crystals, one requires a DFA that is computationally affordable and that provides a satisfactory description of all relevant intra- and intermolecular interactions. Since reliable quantum-chemical reference data is hard to generate for molecular crystals, the performance of DFA+vdW methods is currently evaluated by comparing with experimental structures and extrapolated lattice energies.[24,25]

A molecular crystal composed of the same moieties can have several different crystal-packing motifs or polymorphs. This has far-reaching consequences, as polymorphs can exhibit completely different solubilities, kinetic stabilities, densities, vibrational spectra, nuclear magnetic resonance (NMR) chemical shifts, melting points, conductivities, refractive indices, vapor pressures, elastic constants, heat capacities, etc.[9] It was believed that polymorphism mostly occurred for large and flexible molecules but recently it was suggested by Cruz-Cabeza et al. that polymorphism may be much more common.[26] In the set of crystals they studied, at least one in two molecules had multiple polymorphs. The energy differences between experimentally observed polymorphs are usually less than 4.2 kJ/mol (1 kcal/mol) per molecule but can even be lower than 1 kJ/mol.[26] As a result, to ensure an accurate stability ranking of low-energy polymorphs, calculations with sub-kJ/mol accuracy are necessary. This is already challenging enough, but in addition, experimental crystal structures are always grown and studied at finite temperatures. Thermal effects are usually neglected in state-of-the-art first-principles calculations but can completely change the relative stability and ordering of low-energy polymorphs.[27,28] Furthermore, even if the thermodynamically most stable polymorph at a finite temperature is modeled correctly, it might not crystallize in experiment due to kinetic effects.[29] For example, if the molecular conformation in the thermodynamically stable polymorph is very different from the stable conformation of the isolated molecule, it may not be accessible under the conditions employed in the crystallization experiment. In addition, a predicted polymorph might not be found in experiment because the necessary crystallization experiment has not been performed yet or cannot be performed.[30] Beyond polymorphs of a single-component molecular crystal, we have to deal also with multicomponent systems such as cocrystals, salts, hydrates, and solvates, which will add an additional layer of complexity. The description of all these subtle effects in condensed molecular systems demands a quantum-mechanical first-principles approach if predictive power is desired.

The modeling of response properties of molecular crystals such as vibrational spectra, optical, and elastic properties has also proven to be quite challenging. All of these properties are highly structure dependent and hence also temperature dependent due to thermal expansion. Therefore, accurate THz spectra and elastic constants would require the knowledge of the coordinates and cell parameters corresponding to the desired temperature. Furthermore, these properties are usually calculated by using the (quasi-)harmonic approximation, which means that anharmonic effects due to atomic motion are neglected. However, these effects can be very significant at temperatures close to room temperature.

From this discussion, it is obvious that accurate modeling of molecular crystals from first principles is an intricate task and involves incorporating several effects usually neglected in state-of-the-art calculations. Therefore, we will not only discuss the most important concepts for modeling molecular crystals but also consider the limitations of the approximations employed. First, we will give an overview of the ultimate goal of modeling of molecular crystals, followed by the hard truth of reality. We then discuss how we can predict crystal structures without any experimental information and which first-principles methods can be reasonably applied to realistic systems given current computational power, with a special focus on vdW-inclusive DFT. In the second part of this review, we discuss how we can include

  

thermal and pressure effects in the calculation of structures, energetics, and response properties.

## WHERE WE WOULD LIKE TO BE—A DAY DREAM

Ideally, we would like to predict the three-dimensional (3D) crystal structure and corresponding solid-state response properties of a given molecule for desired experimental conditions, which could then be used to guide or even predict experiments. For example, in the context of crystal engineering we would then be able to propose molecular crystals that show certain desirable properties under specific thermodynamic conditions. As a result, we would like to know the complete crystal energy landscape for any temperature and pressure, i.e., the complete crystalline phase diagram calculated from first principles. This would provide information about the thermodynamic stability of different polymorphs for a given molecular crystal.

In principle, given sufficient computational resources, the exact energy of molecular crystals could be calculated in the nonrelativistic limit by using the full configuration interaction (full CI) method,[31,32] which considers Slater determinants of the ground state and *all* possible excitations at 0 K. Obviously, it is imperative to employ an electronic-structure method that is size extensive and capable of yielding analytical expressions for the atomic forces (such as full CI, coupled cluster, or infinite-order perturbation theories). Then, temperature and pressure effects are accessible via molecular dynamics (MD) simulations.[33] As most experiments are performed at constant temperature and pressure, the isothermal–isobaric (NPT) statistical ensemble should provide a picture close to reality. However, this ensemble is computationally demanding, since the volume of the cell is not constant during the simulation. Ideally, we would perform the MD simulation with a supercell large enough to capture all long-range effects and potentially to model small defects in the crystal. In order to correctly capture the quantum nature of the nuclei, it is also necessary to use path-integral MD, since standard MD describes the dynamics of the nuclei only on a classical level. In addition, we would like to explicitly include crystallization conditions in crystal-structure prediction calculations and explore kinetic effects. Kinetics could be studied by simulating crystal growth by using a kinetic Monte Carlo algorithm.[34–36] For a detailed discussion on kinetic effects, the reader is referred to Refs 30,37–39.

These simulations would provide us with the structure of the most stable polymorph of a certain molecule under specific thermodynamic conditions. Vibrational spectra could be obtained from the MD simulations via a Fourier transform of the velocity autocorrelation function. The same is true for elastic properties. Optical and dielectric properties, as well as NMR chemical shifts and other properties, can be calculated based on a time-averaged static structure.

## WHERE WE ARE—BACK TO REALITY

Unfortunately, the previously described MD simulations are currently impossible to perform with first-principles methods for realistic systems, especially for crystals of flexible molecules. The necessary size of the simulation cell and the required timescale for meaningful MD simulations is currently far beyond available computational resources. We expect that this kind of simulations will not be possible for many years for the majority of realistic systems.

Therefore, geometry optimizations are usually done without explicitly including thermal or zero-point effects. The thermal expansion of a molecular crystal can be approximated by using the so-called quasi-harmonic approximation (QHA). With this approach, which will be discussed in detail below, one can capture about 80% of the actual thermal expansion. To our knowledge, kinetic effects have not been studied so far in crystal-structure prediction calculations at a fully first-principles level. However, this is only due to the lack of the necessary computational power to perform these calculations. In principle, the kinetic Monte Carlo method would be appropriate for modeling these effects.[34–36] In addition, most lattice-energy calculations involve only electronic energies and nuclear repulsion, with free-energy contributions commonly neglected. Vibrational free energies can be approximated in the harmonic limit, and with this approach we can expect an accuracy for lattice energies up to 4.2 kJ/mol.[25] Part of the anharmonic contributions can be included by using the QHA, where thermal expansion is considered.[40,41] Recently, a so-called vibrational self-consistent field (VSCF) method was developed, in which anharmonicity is explored by calculating several points along normal-mode displacements.[42] This method has already been applied to solid molecular hydrogen[43] and ice.[44]

Furthermore, the calculation of first principles vibrational spectra is typically limited to the harmonic approximation (HA), but the volume dependence of vibrational modes can at least be

  

approximated by the QHA. While this provides reasonable vibrational frequencies at very low temperatures, the low-frequency modes differ significantly from experimental measurements at higher temperatures due to large anharmonicities.[45] However, we stress that this approach is still much more accurate than performing molecular-dynamics simulations with traditional force fields because the accuracy of force-field forces is in this case usually not sufficient for modeling response properties. Mechanical and optical properties are also usually modeled at the minimum of the electronic potential-energy surface (PES) or with the quasi-static approach, i.e., fixing the unit cell to the experimental volume for a certain temperature.[46] Note that the calculation of optical properties is essentially only possible with first-principles methods because this requires consideration of excited electronic states.

Despite all these remaining challenges, first-principles methods have already yielded significant new insights into molecular crystals. The most recent crystal-structure prediction blind test[47] has shown that first-principles methods can now be successfully applied for pharmaceutically relevant flexible molecular crystals, salts, and hydrates, and that they provide better structures and stabilities than force-field approaches. Furthermore, it was shown by Reilly and Tkatchenko that a high-level vdW-inclusive DFT method is able to describe the relative enthalpy and entropy of the two known polymorphs of aspirin correctly, offering a resolution for a long-standing controversy regarding the metastability of form-II aspirin.[27] In addition, Schatschneider et al. have shown that vdW-inclusive DFT is able to describe temperature-induced phase transitions between molecular crystal polymorphs of tetracyanoethylene in excellent agreement with experimental data.[48]

## INTERMOLECULAR INTERACTIONS IN MOLECULAR CRYSTALS

As molecular crystals consist of molecular moieties, the cohesion within the crystal arises from noncovalent or intermolecular interactions, with the majority of their properties also governed by intermolecular interactions. Therefore, it is necessary to understand and properly model these many different types of interactions in an accurate and balanced manner. In general, we can loosely distinguish between four different types of noncovalent interactions between closed-shell molecules: electrostatics, exchange repulsion, induction, and dispersion.[49] We can understand these interactions in a textbook picture based on perturbation theory[50] as follows: electrostatics describes the static Coulomb interaction between fixed molecular charge distributions, i.e., the interaction between permanent multipoles with the leading terms being dipole–dipole, dipole–quadrupole, quadrupole–quadrupole, etc. The exchange repulsion is comprised of two effects. The first one is an attractive interaction, which arises due to the fact that electrons can move over both molecules at short intermolecular distances, and the second effect is a result of the Pauli exclusion principle, which leads to the existence of a repulsive force between electrons of the same spin. Overall, the exchange repulsion is dominated by the second effect and is therefore repulsive. Induction describes the interaction between permanent and induced multipoles. Finally, the dispersion term describes the interaction between instantaneously created multipoles and induced multipoles, i.e., zero-point fluctuations of electrons in one molecule create an instantaneous multipole moment, which can then induce a multipole moment in another molecule. The dispersion interaction is ubiquitous because it does not require the existence of permanent multipole moments.

As we wish to discuss in this review the modeling of molecular crystals with density functional methods, we also provide a slightly different interpretation of intermolecular interactions based on electron densities (see Figure 1). In all first-principles calculations, the electron density of a system is obtained via an iterative self-consistent field (SCF) approach.[31] At the beginning of the SCF procedure, a static density is initialized, typically using atomic-charge information. This initial stage can be viewed as electrostatics. When electron clouds overlap, the exchange of electrons becomes possible. The Pauli principle requires that the total wave function is antisymmetric with respect to exchange of electrons of the same spin. The adaptation of the wave function is connected with an energy loss and therefore

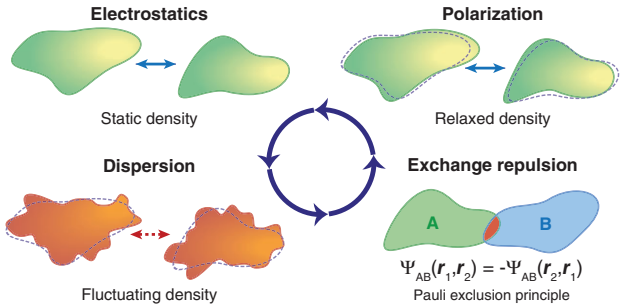


**FIGURE 1** | Schematic representation of intermolecular interactions.

  

repulsive interaction. As the SCF cycle progresses, the electron densities of the atoms/molecules relax in response to the surrounding charge distributions. This effect can be understood as polarization or induction. The three effects discussed so far would describe the picture of intermolecular interactions within Hartree–Fock theory and semi-local DFAs. For any method accounting for long-range electron correlation energy, the instantaneous electronic fluctuations lead to an additional modification of electron densities compared to electronic mean-field models. The intermolecular interaction arising due to this effect can be loosely interpreted as dispersion. It has been shown by Ferri et al.[51] that long-range vdW (dispersion) interactions can significantly modify the electron density and related electronic properties. In general, all of the discussed effects (repulsion, electrostatics, polarization, and dispersion) are intimately linked together and there is no unambiguous way to separate them in practice, especially for extended crystals.

The complexity of describing all of the discussed interactions on equal footing makes the use of first-principles methods imperative for an accurate modeling of molecular crystals. However, most calculations are still carried out with empirical force fields that often only describe electrostatics and employ rather crude models for Pauli repulsion and dispersion interactions. Typically, polarization is treated only poorly or neglected completely by these classical models, although polarizable force fields have been developed. While fully self-consistent first-principles methods can also capture complex nonadditive effects between exchange-repulsion, electrostatics, polarization, and dispersion, force fields treat these terms only in an additive fashion.

As discussed by Dobson and Gould,[52] the term *van der Waals (vdW) interactions* often has varying meaning in different communities. In chemistry, the sum of all intermolecular interactions is often termed *vdW interactions*, whereas in solid-state physics, it usually describes effects due to correlations between electronic fluctuations, which correspond to the dispersion interactions defined above. We will adopt the latter definition throughout this review. Within molecular crystals, vdW interactions can dominate the cohesive energy given their long-range nature and ubiquity. However, hydrogen bonds[53] and also halogen bonds play a very important role in crystal engineering because of their directional-dependent attraction at short range. This can be used to control structural motifs in the formation of molecular crystals. The nature of intermolecular interactions within hydrogen- and halogen-bonded systems was recently analyzed in Refs 54–56 using symmetry-adapted perturbation theory.[57,58]

We now proceed to discuss how one can predict crystal structures and properties of molecular crystals by combining a hierarchy of modeling approaches for the increasingly accurate description of intermolecular interactions.

## PREDICTING CRYSTAL STRUCTURES AND PROPERTIES

For the modeling of experimentally known molecular crystals, the determined crystal structure is often used as starting point for theoretical calculations. Usually, this experimental structure is reoptimized with the first-principles method of choice and all properties are calculated from that structure. However, as we want to predict certain properties of molecular crystals prior to experiment, we need to determine the most stable crystal structure of a certain molecule from scratch. Since 1999, the Cambridge Crystallographic Data Centre (CCDC) has organized several crystal-structure prediction (CSP) blind tests.[47,59–63] In these blind tests, the participants were required to predict the experimentally determined crystal structures of several molecules based only on the knowledge of the two-dimensional (2D) chemical diagram. Most groups used force-field approaches but the number of first-principles contributions (especially DFA+vdW) is increasing. Since 2009, one method has correctly predicted most of the target crystal structures.[47,62,63] However, the accurate stability ranking of polymorphs still remains a challenge, with only the most sophisticated many-body dispersion (MBD) method leading to a significantly improved rank order prediction.[47] In addition, thermal effects and kinetic effects are still mostly neglected in current crystal-structure prediction calculations. Kinetic effects due to crystallization conditions in experiments can restrict the diversity of accessible polymorphs, while thermal effects can radically change the relative stabilities of polymorphs.

Whenever the crystal structure is not known experimentally, we have to start with a 2D chemical diagram of the target molecule. The procedure for finding the lowest-energy polymorph can be divided into three basic steps, which we will briefly mention in the following sections. For a more detailed description of this process, the reader is referred to Ref 37. All properties of molecular crystals are highly dependent on the crystal structure. Therefore, properties can be calculated after we have obtained the most stable crystal structure. The calculation of

  

vibrational and elastic properties will be discussed in the *Addressing the Temperature and Pressure Gap* section.

## Step 1: Generating Molecular Conformations

As molecular crystals consist of noncovalently bound molecular entities, a reasonable starting point is to calculate the most stable conformer of a molecule in the gas phase. In many instances, this conformer will already be a good estimate of the conformation adopted within the crystal, especially for rigid molecules. However, when a molecule can form intermolecular hydrogen bonds, the additional stabilization of these can lead to significant changes in conformation to accommodate their formation. This is especially an issue for molecules that form intramolecular hydrogen bonds. Furthermore, several rotations about single bonds can occur in flexible molecules that do not dramatically change the conformational energy, e.g., rotation of alkyl linkers or phenyl groups.

It is also possible that the most stable geometry in the crystal is a different tautomer compared to the most stable geometry in vacuum. For example, barbituric acid was believed to occur only in the keto form. Recently, a polymorph featuring the enol form was found and is more stable at room temperature than all previously known polymorphs.[64]

## Step 2: Crystal-Packing Arrangement

In the second step, a large number of different putative crystal-packing arrangements must be calculated. This task is highly nontrivial, as we do not know how many molecules are in the unit cell or which space group the molecule will crystallize in. Even if we have only one kind of molecule in the crystal and if the conformation of all molecules is the same, the size of the crystallographic space to be covered is tremendous. One important parameter in this search is the number of molecules in the asymmetric unit of the unit cell ($Z'$), i.e., the number of molecules that are necessary in order to generate all atomic positions within the unit cell through symmetry operations. In most crystal-structure searches, only $Z' = 1$ structures are considered but for several systems, it can easily be greater than 1. However, the sampling for these less symmetric structures vastly increases the number of possible crystal structures that need to be considered and therefore significantly increases the computation time. Hence, for every crystal-structure prediction, one has to find a balance between accuracy and cost of the search. In a first approximation, gas-phase molecular structures are used to create initial crystal-packing geometries. For flexible molecules, several torsion angles must be considered for rotatable bonds, which vastly increase the complexity of the crystal-structure prediction.[65,66] In addition, one may have to consider also the possibility of hydrates, solvates, and different stoichiometry. In some cases, it can also be difficult to distinguish between salts and cocrystals, which often only differ in the position of a proton. Such systems might therefore require considering both possibilities.

## Step 3: Stability Ranking

Once a sufficiently large set of crystal-packing arrangements has been created, one has to rank all of them according to a certain measure of stability. Usually, this is done by calculating the lattice energy $E_{\text{latt}}$, which is given by

$$E_{\text{latt}} = \frac{E_{\text{cryst}}}{Z} - E_{\text{gas}} \tag{1}$$

where $E_{\text{cryst}}$ is the energy of the crystal unit cell, $E_{\text{gas}}$ is the energy of one isolated molecule in the lowest-energy gas-phase conformation, and $Z$ is the number of molecules in the unit cell. It describes the energy of formation of a molecular crystal from infinitely separated molecules in their gas-phase minimum-energy conformation, or in other words, the molecular energy gained by forming a crystal. If a crystal is stable, the lattice energy has a negative sign. Typically, lattice-energy calculations do not include any thermal effects, i.e., only the electronic energy and the nuclear-repulsion energy are considered.

Ideally, all calculations should be done by first-principles methods to ensure accurate modeling of conformations and crystal structures through the whole CSP process. However, the proper sampling of the crystal-structure search space requires a large number of calculations. Therefore, it is common to use the following approach: at first, the molecular conformation (step 1) is optimized with a first-principles method, such as DFT, followed by the generation of parameters for a first-principles-derived force field. Next, a large number of possible crystal-packing arrangements are created based on the DFT-optimized molecular structures (step 2) and they are ranked by their stability according to the force-field lattice energy (step 3). After this initial ranking, an appropriate number of low-energy structures can then be reoptimized and reranked with a hierarchy of increasingly accurate methods, starting with a first-

  

principles-derived force field up to high-level first-principles methods. If done properly, this eventually leads to the most-stable crystal structure with the final method of choice.

### Step 4: Calculation of Properties

The stable structure is merely a proxy for calculating a range of properties desirable in actual solid-state applications. With the structure determined in Step 3, we are now able to calculate a variety of response properties. Vibrational properties can be calculated within the HA by determining the forces due to finite atomic displacements. This provides information about vibrational modes of the molecular crystal, including internal modes and phonon modes. With that, one can obtain THz fingerprint spectra [low-frequency infrared (IR) spectra], free energies at finite temperatures, and heat capacities at constant volume. The mechanical stability of a molecular crystal can be assessed via elastic constants and moduli. These quantities are calculated by determining the stress tensor on several strained unit cells. All these properties will be discussed later on in this review. In addition, we can also calculate charge-transport properties of molecular crystals. Recently, Motta and Sanvito[67] have proposed a model for calculating the charge mobility of a molecular crystal at specific temperatures using data from lattice-dynamics calculations. This model constructs an effective tight-binding Hamiltonian that describes the electron–phonon coupling. The NMR chemical shifts of molecular crystals can be calculated from the chemical-shielding tensor, the components of which are the second derivatives of the energy with respect to an external magnetic field and the nuclear magnetic moment. Most calculations use the so-called gauge-including projector augmented wave (GIPAW) method.[68,69] Recently, a fragment-based method has also been developed by Hartman et al.[70] Chemical shifts can be used to distinguish between different polymorphs or to assign peaks in experimental NMR spectra.[70,71] However, the differences in chemical shifts between polymorphs are small and sensitive to the crystal-structure geometry, which makes accurate modeling especially challenging.

It is important to remember, however, that the final structures from a crystal-structure prediction calculation typically do not include any contribution from thermal expansion or motion. To incorporate these effects the QHA can be used to determine finite-temperature lattice constants, which will be discussed in the *Addressing the Temperature and Pressure Gap* section. It can also be used to model an approximate temperature dependence in vibrational modes, elastic constants, and NMR shifts. In addition, it enables the calculation of thermal expansion coefficients or heat capacities at constant pressure.

## CALCULATING CRYSTAL STRUCTURES AND LATTICE ENERGIES

### Method Overview

There is a range of methods that can be used to calculate energies, geometries, and response properties of molecular crystals. Before considering first-principles methods, it is worth noting that force-field methods are indispensable for crystal-structure prediction calculations. Owing to their low computational cost, they can be used to rapidly evaluate all of the generated crystal-packing arrangements and provide a preselection for first-principles methods. However, even the most recent force fields do not provide the reliability and accuracy of high-quality first-principles calculations. For molecular crystals, first-principles-derived force fields are more successful than conventional force fields because they are fitted especially for the molecule being studied and therefore usually describe lattice energies far more accurately than conventional force fields.[72,73] Semi-empirical density functional tight-binding methods can also be used for preselection of structures, which are then subsequently investigated with first-principles methods.[74,75] However, the parametrization of these methods can lead to problems for flexible molecular crystals with a large number of freely rotatable functional groups. The relative stability ranking of conformations with these methods can also be poor, giving spurious results in CSP calculations.[47]

In recent years, various first-principles methods have been developed for modeling extended molecular crystals. We will briefly mention important classes of methods. For a more in-depth discussion, the reader is referred to Ref 71. We begin with periodic DFT. Most traditional DFAs lack the ability to describe long-range correlation energy, which can lead to completely wrong lattice energies and geometries for molecular crystals. In recent years, this deficiency has been addressed by developing models for vdW interactions that are added to the total DFT energy[16–20] (which are then termed vdW-inclusive methods) and also by the development of nonlocal functionals.[76] These methods will be discussed in more detail in the next section. As a result of these recent developments, DFT is becoming the method of

  

choice for molecular crystals, as it provides a good balance between accuracy and computational cost.

Periodic post Hartree–Fock calculations have also recently become possible for small molecular crystals. Periodic local second-order Møller–Plesset perturbation theory (MP2) has successfully been applied to several small molecular crystals including carbon dioxide,[77] urea,[78] and ammonia.[77] Furthermore, Grüneis et al. developed a periodic MP2 method based on a plane-wave basis set.[79] This development is encouraging, however, these calculations are much more time consuming than DFT calculations and require much larger basis sets for converged results. Another high-level first-principles method is diffusion QMC, which is mainly used for benchmarking, as the required computation time scales rapidly with system size. The largest reported calculation so far is that of the energy difference between two polymorphs of diiodobenzene.[80,81] However, converging small energy differences between polymorphs with QMC is challenging due to finite-size effects and inherent statistical sampling errors.

Finally, the last important class of methods are the so-called fragment methods. In these methods, the total energy of a molecular crystal is decomposed into molecular energies $E_i$ (monomers), the interaction between two molecules $\Delta E_{ij}$, three-molecule interactions $\Delta E_{ijk}$, etc.

$$E_{\text{tot}} = \sum_i E_i + \sum_{ij} \Delta E_{ij} + \sum_{ijk} \Delta E_{ijk} + \sum_{ijkl} \Delta E_{ijkl} + \cdots \quad (2)$$

This has the advantage that the overall computational cost is lowered substantially, which enables calculations with high-level wave function-based methods. For example, Yang et al. were able to calculate the lattice energy of the benzene crystal in this way with a coupled cluster method with perturbative triple excitations.[82] Interactions up to four-molecule terms are necessary to converge the lattice energy.[83] Heit et al. applied the fragment-based hybrid many-body interaction (HMBI) model to crystalline carbon dioxide.[40,84] This method calculates the intramolecular energy and the short-range two-body energy with either MP2 or coupled cluster singles and doubles with perturbative triples [CCSD(T)], and the long-range two-body and remaining many-body interactions by using the AMOEBA polarizable force field. However, MP2 suffers from the problem that it overestimates lattice energies, especially for dispersion-bound systems with $\pi$-stacking.[85] Another important fragment method is symmetry-adapted perturbation theory.[50,57] With this method, one can decompose interaction energies between molecules into electrostatics, exchange, induction, and dispersion contributions. For a detailed description of its application to molecular crystals, the reader is referred to Ref 86.

## vdW-Inclusive DFT

In vdW-inclusive DFT, the missing dispersion energy $E_{\text{disp}}$ is calculated *a posteriori* and then added to the total DFT energy of the DFA used. Most pairwise schemes have the following general form

$$E_{\text{disp}} = -\sum_{i>j} f_{\text{dmp}} \frac{C_6^{ij}}{R_{ij}^6}, \quad (3)$$

where $R_{ij}$ is the interatomic distance, $C_6^{ij}$ describes the dipole–dipole dispersion coefficient between atoms $i$ and $j$, and $f_{\text{dmp}}$ is a damping function. For a detailed discussion of the importance of the used damping function, the reader is referred to Ref 87. The dispersion coefficients are related to the atomic polarizabilities. This approach is used, for example, for the DFT-D2 method[16] and the Tkatchenko–Scheffler (TS) method.[19] In the D2 scheme fixed empirical dispersion coefficients are used, while in the TS scheme, they are directly derived 'on the fly' from the calculated electron density. Furthermore, the TS and the related MBD method are explicit density functionals and hence permit investigation of the effect of vdW interactions on all properties of interest beyond structures and stabilities of molecular crystals.[51,88]

The dispersion interaction can be expressed in a multipole expansion. The D2 and TS schemes include only dipole–dipole interactions. Therefore, one possibility is to augment them by dipole–quadrupole interactions, adding a $C_8^{ij}/R_{ij}^8$ term. This is done in the DFT-D3 method,[17] where the fixed dispersion coefficients were replaced by coefficients dependent on atomic coordination. Another important dispersion model is the exchange-dipole moment (XDM) model,[18,89,90] which is also density dependent and includes pairwise interactions up to quadrupole–quadrupole interactions.

However, dispersion interactions are not pairwise additive and therefore many-body interactions have to be considered as well.[91] In the case of DFT-D3, the many-body interactions are approximated by the lowest-order three-body term (Axilrod-Teller-Muto), which describes the interaction between three instantaneous dipoles. In 2012, Tkatchenko et al. developed the so-called many-body dispersion (MBD) method, which considers many-body dipolar interactions up to infinite order.[20] The MBD method

  

also includes electrodynamic response (dielectric screening) effects by a self-consistent screening of atomic polarizabilities. These effects are especially important for extended systems like molecular crystals because the presence of the crystal field changes polarizabilities considerably compared to isolated molecules. The MBD dispersion energy (long-range correlation energy) is given by

$$E_{\mathrm{MBD}} = \frac{1}{2\pi}\int_0^\infty \mathrm{d}\omega\, \mathrm{Tr}[\ln(\mathbf{1}-\mathbf{AT})] \qquad (4)$$

where **A** is a diagonal $3n \times 3n$ matrix containing the isotropic atomic polarizabilities and **T** is the dipole–dipole coupling tensor. This expression is equivalent to diagonalizing a model Hamiltonian of coupled isotropic quantum harmonic oscillators. For a more in-depth discussion of the MBD method, the reader is referred to Refs 91–93.

In contrast to small gas-phase molecules, dispersion interactions can extend over large distances in molecular crystals. This is illustrated in Figure 2 for a cubic deutero ammonia ($ND_3$) and a hexamethylbenzene (HMB) crystal. The figure shows the convergence of the vdW lattice energy (per molecule) with respect to a cut off radius $r_{\mathrm{cut}}$, i.e., the completely converged energy is set to zero. In the case of the pairwise dispersion approach (TS), interactions between atoms are only considered if the interatomic distance is less than or equal to $r_{\mathrm{cut}}$. In the MBD case, interactions are only included in the dipole–dipole tensor if the interatomic distance between two atoms is less than or equal to $r_{\mathrm{cut}}$. In addition, the coupling between the harmonic oscillators is considered within a cubic supercell of lattice constant $a = r_{\mathrm{cut}}$. It can be seen that the coupling of the harmonic oscillators (MBD) leads to a significantly slower convergence for both systems than the pairwise dispersion energy (TS). In order to converge the lattice energy of HMB within 0.5 kJ/mol, one needs to consider distances of roughly 22 Å for TS and already around 35 Å for MBD. This shows immediately that we are missing important collective effects by only considering pairwise interactions. In contrast, MBD considers many-body interactions up to infinite order. We mention in passing that molecular-crystal polymorphs often have similar short-range order and interactions, and are therefore sometimes only distinguishable at relatively large distances between molecules. It is precisely at these distances that many-body screening effects are largest; hence, pairwise dispersion corrections are frequently unable to capture the subtle energetic difference between polymorphs. Both $ND_3$ and HMB are rather symmetric (cubic) molecular crystals. For more complex geometries with lower symmetry, we expect the range of many-body vdW interactions to be even longer, as for example exemplified by the analysis of vdW interactions in nanostructured materials.[94,95]

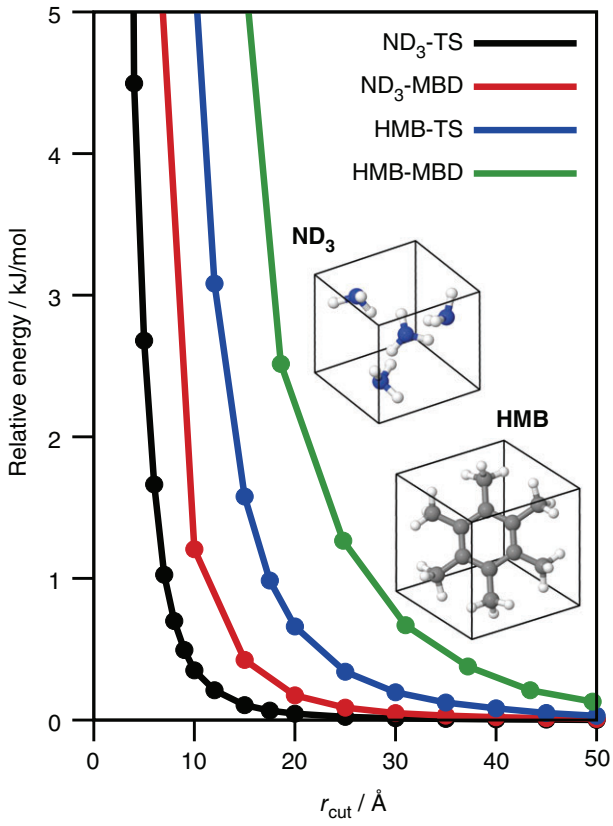


**FIGURE 2** | Convergence of the pairwise (TS) and MBD vdW lattice energy with respect to the dipole–dipole cut off radius and MBD supercell cut off radius for $ND_3$ and HMB. HMB, hexamethylbenzene; MBD, many-body dispersion; $ND_3$, cubic deutero ammonia; TS, Tkatchenko–Scheffler; vdW, van der Waals.

## Lattice-Energy Benchmarks

For molecular dimers, benchmarks of interaction energies can be easily made by comparing with CCSD(T) calculations at the basis-set limit using several databases. However, such theoretical benchmark sets are unfortunately not available for molecular crystals. The best solution is to compare calculations to experimental sublimation enthalpies. One very well-studied system is the benzene crystal. The experimental lattice energy is $-55.3 \pm 2.2$ kJ/mol.[82] The highest-level first-principles result available was calculated with a fragment coupled cluster approach by including two, three, and four-molecule interactions, yielding a lattice energy of $-55.9 \pm 0.76 \pm 0.1$ kJ/mol.[82] The fragment HMBI model based on CCSD(T) provides a lattice

  

energy of −53.0 kJ/mol[96,97] and the periodic local MP2 approach leads to a lattice energy of −56.6 kJ/mol.[98] This shows that all calculations using post-Hartree-Fock methods provide excellent agreement with experiment for the benzene crystal. In contrast, the widely used density functional B3LYP without any dispersion correction yields a lattice energy of only −15.9 kJ/mol, which corresponds to an error of almost 40 kJ/mol.[99] Therefore, it is imperative to include proper vdW interactions in DFT calculations. The Perdew-Burke-Ernzerhof (PBE) DFA[100] supplemented by the MBD and the XDM methods yield lattice energies of −55.0 and −49.5 kJ/mol, respectively.[24,25] In addition, the lattice energy calculated with PBE+D3 with and without three-body terms amounts to −51.0 and −54.8 kJ/mol, respectively.[101] It can be seen that most vdW-inclusive DFT methods provide lattice energies for the benzene crystal that are in excellent agreement with the experimental value.

In 2012, Otero-de-la-Roza and Johnson assembled the C21 benchmark set containing 21 molecular crystals ranging from dispersion-bound to hydrogen-bonded systems.[24] The experimental sublimation enthalpies were back corrected for vibrational contributions, yielding benchmark values for 0 K lattice energies. This benchmark set was extended and refined by Reilly and Tkatchenko, yielding the X23 benchmark set.[25] The relative error in the lattice energies compared to the benchmark values is shown in Figure 3 for the PBE and PBE0 DFAs supplemented by the TS and MBD methods.

It can be seen that MBD produces systematically more accurate lattice energies than TS. The largest difference between TS and MBD is found for the vdW-bound systems. In addition, switching from the generalized gradient approximation (GGA) functional PBE to the PBE0 hybrid functional leads to a consistently better description of the lattice energy. The TS method consistently overestimates lattice energies, giving a mean absolute error (MAE) of 10.0 kJ/mol for PBE0+TS. For PBE0+MBD, the MAE amounts to only 3.9 kJ/mol, placing it within the 4.2 kJ/mol (1 kcal/mol) window of chemical accuracy. The D3 dispersion correction has also been tested for several functionals with the X23 benchmark set.[101] The best performance was achieved for TPSS-D3 without three-body terms, also yielding an MAE of 3.9 kJ/mol.

Nyman et al.[102] have recently studied the accuracy of several force fields widely used in crystal-structure prediction calculations for the X23 benchmark set. The resulting deviations in lattice energies are around 2–3 times larger than the best vdW-inclusive first-principles methods. These deviations are reasonable in the context of using such force fields in the intermediate stages of crystal-structure prediction calculations but not sufficient for correctly predicting the rank ordering of polymorphs and it should also be noted that they are parameterized for a limited number of atom types and environments and are therefore not very transferable.

All of the above benchmarks are for absolute lattice energies. However, for crystal-structure prediction calculations, relative energies are required. The C21 and X23 test sets include two polymorphs of oxalic acid. Experimentally,[24,25,103,104] the $\alpha$ polymorph is slightly more stable than the $\beta$ form, by 0.2 kJ/mol. The DFA methods discussed above yield energy differences ranging from about −4 kJ/mol to 4 kJ/mol. For PBE0+TS, the $\beta$ form is more stable by about 1.5 kJ/mol, while PBE0+MBD predicts that the $\alpha$ form is more stable by about 1 kJ/mol, which is consistent with experiment. In addition, the relative stability of three glycine polymorphs has been studied for several vdW-inclusive DFAs by Marom et al.[105] Only PBE0+MBD was able to capture correctly the qualitative stability ranking, while PBE+TS, PBE0+TS, and PBE+MBD yielded a different qualitative picture. The error in the calculated relative energies amounts to about 1 kJ/mol for PBE0+MBD. All these benchmarks suggest that high-level vdW-inclusive DFAs are necessary for accurate relative stabilities and that the stability ranking of polymorphs within an energy window of 1–2 kJ/mol remains a challenge. It also is important to remember though that the experimental reference values for polymorph and absolute stabilities are associated

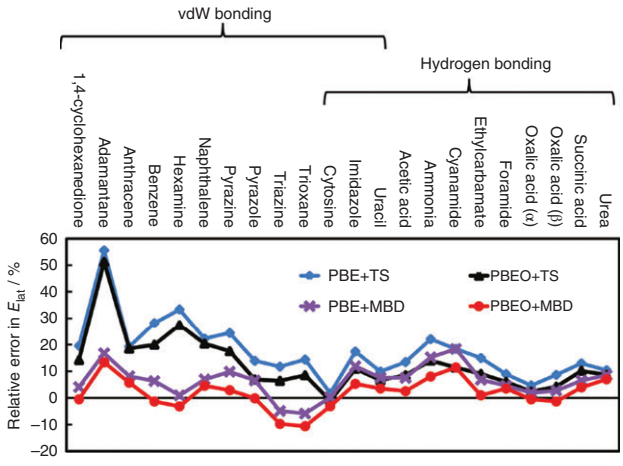


**FIGURE 3** | Relative error in the calculation of lattice energies for 22 molecular crystals for PBE+TS, PBE+MBD, PBE0+TS, and PBE0+MBD calculations. (Reprinted with permission from Ref 25. with the permission of AIP Publishing) MBD, many-body dispersion; TS, Tkatchenko–Scheffler.

  

with an uncertainty, and that the often-used back correction of experimental sublimation enthalpies also introduces an additional uncertainty in these benchmarks.

## Geometry Benchmarks

As with lattice energies, there is no high-level first-principles benchmark set available for geometries of molecular crystals. Therefore, we have to compare the theoretically optimized structures with experimental crystal structures, usually measured by X-ray diffraction. However, all experimental structures are measured at finite temperatures, whereas theoretical geometry optimizations correspond to 0 K and also do not include zero-point effects. Most molecular crystals expand with increasing temperature and even the zero-point vibrations alone can lead to a volume expansion of about 3%, which will be shown later on for phase-I ammonia. One approach to combat this is to benchmark theoretical structures against the lowest-possible temperature structure available in experiment, minimizing the influence of thermal effects. The lattice vectors obtained with PBE+TS and PBE+MBD optimizations for a subset of the X23 test set show mean relative errors of –0.55 and –0.75%, respectively.[25] Moellmann and Grimme[101] studied the structures of the C21 set by using PBE+D3 and TPSS+D3, yielding mean relative errors in the cell volume of –1.1 and –2.3%, respectively. Calculated structures usually show a smaller volume compared to experiment, most likely due to neglecting thermal expansion.[25,106] Schatschneider et al.[106] studied the structures of a large set of crystalline polycyclic aromatic hydrocarbons with PBE+TS, yielding on average an error of about ±2% for the lattice vectors. A comparison of the calculated densities with experimental values is shown in Figure 4. Most of the room temperature experimental densities agree within 5%, with the calculated densities, while for lower temperatures, the agreement improves to an average deviation of 2.3%.[106] The main reason for the overestimation of the densities is again the neglect of any temperature or zero-point effect in the geometry optimization. The most-recent blind test of crystal-structure prediction methods[47] has also shown that several first-principles methods are able to predict structures in very good agreement with experimental geometries and, in general, with a higher accuracy than force-field approaches.

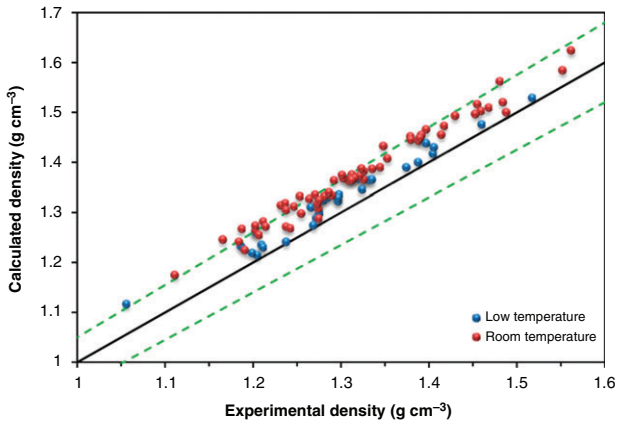


**FIGURE 4** | Calculated versus experimental densities for 91 polycyclic aromatic hydrocarbons. Structures obtained at room temperature are shown in red and structures obtained below room temperature are shown in blue. The black line marks perfect agreement, while the green dotted lines mark a deviation of ±5%. (Reprinted with permission from Ref 106. Copyright 2014 American Chemical Society).

## ADDRESSING THE TEMPERATURE AND PRESSURE GAP

The lattice energies discussed so far contain only total energies (electronic and nuclear repulsion) calculated with a first principle method; from now on abbreviated with $E_{tot}$. These energies do not depend on temperature and pressure and are therefore only valid at a temperature of 0 K and a pressure of 0 bar. Strictly speaking, we are not even describing 0 K correctly, as vibrational zero-point energies are missing. While this might sometimes be a reasonable approximation for modeling small isolated molecules in vacuum, temperature and pressure effects can be crucial for the accurate modeling of molecular crystals.

In order to include temperature effects, we need to calculate the Helmholtz free energy $F(T, V)$, given by

$$F(T,V) = E_{tot}(V) + F_{vib}(T,V) \quad (5)$$

where $F_{vib}(T, V)$ is the vibrational free energy due to the nuclear motion on the Born–Oppenheimer energy surface, $T$ is the temperature, and $V$ is the unit-cell volume of the molecular crystal. There are additional contributions to $F(T, V)$, such as the electronic free energy[107] and magnetic contributions. However, these effects can normally be neglected for insulating molecular crystals. Furthermore, we assume that we are dealing with a perfectly periodic molecular crystal. The existence of defects or disorder would also introduce additional terms in $F(T, V)$. The effect of pressure can be readily included by calculating the Gibbs free energy of the crystal:

$$G(p,T,V) = F(T,V) + pV \tag{6}$$

where $p$ is an external hydrostatic pressure acting on the unit cell.

In the following subsections, we will discuss the basics of approximations for including thermal effects with the aid of a simple model system phase-I deutero ammonia ($ND_3$). In addition, we also discuss how vdW interactions influence the results. All calculations for the model system were performed within the all-electron DFT code FHI-aims,[108–111] using the tight species default settings and phonopy, a code for phonon calculations.[112]

## The Harmonic Approximation

The simplest way to calculate the Helmholtz free energy is the so-called harmonic approximation (HA). In principle, the calculation of $F_{vib}$ requires the knowledge of the total PES, which is a $3n$-dimensional object, where $n$ is the number of atoms in the unit cell. In the HA, the PES is expressed around the equilibrium geometry with coordinates $\boldsymbol{R}_{eq}$ by a second-order Taylor expansion

$$E(\boldsymbol{R}_{eq} + \Delta\boldsymbol{R}) = E(\boldsymbol{R}_{eq}) + \sum_i \frac{\partial E}{\partial \boldsymbol{R}_i}\Delta\boldsymbol{R}_i + \frac{1}{2}\sum_{i,j}\frac{\partial^2 E}{\partial \boldsymbol{R}_i \partial \boldsymbol{R}_j}\Delta\boldsymbol{R}_i\Delta\boldsymbol{R}_j + \mathcal{O}(\Delta\boldsymbol{R}^3) \tag{7}$$

where $E(\mathbf{R}_{eq})$ is the total energy of the equilibrium geometry. The first-order term vanishes since the forces are zero at a local minimum of the PES. The second-order term will provide us with the harmonic force constants $\Phi_{ij}$

$$\frac{\partial^2 E}{\partial \mathbf{R}_i \partial \mathbf{R}_j} = -\frac{\partial \mathbf{F}_j}{\partial \mathbf{R}_i} = \Phi_{ij} \tag{8}$$

which build up the Hessian matrix, or for periodic systems the so-called *dynamical matrix*.[113] All effects arising from higher-order terms in the Taylor expansion in Eq. (7) are called *anharmonic effects* and are completely neglected in the HA.

The harmonic force constant $\Phi_{ij}$ describes the change of the force on atom $j$ when displacing atom $i$. The dynamical matrix is typically calculated numerically by finite differences, but is also accessible by using density functional perturbation theory.[114] The eigenvalues of the dynamical matrix are the phonon frequencies $\omega$ (vibrational frequencies in nonperiodic systems) and the eigenvectors describe the corresponding phonon modes. The complete dynamics of the harmonic system is described by $3n$-independent quantum harmonic oscillators; one for each phonon mode.

As the HA only approximates the PES around the equilibrium structure with a corresponding unit-cell volume $V_{eq}$, the harmonic Helmholtz free energy $F^{HA}$ does not have an explicit volume dependence and can be expressed as

$$F^{HA}(T) = E_{tot} + F^{HA}_{vib}(T) \tag{9}$$

with

$$F^{HA}_{vib}(T) = \int d\omega g(\omega)\frac{\hbar\omega}{2} + \int d\omega g(\omega) k_B T \ln\left[1 - \exp\left(-\frac{\hbar\omega}{k_B T}\right)\right] \tag{10}$$

where $g(\omega)$ is the phonon density of states (pDOS), i.e., the number of vibrational states at a certain frequency. The first integral in Eq. (10) describes zero-point vibrations, which are present in every quantum system even at 0 K, while the second integral describes thermally-induced vibrations and accounts for vibrational entropy. Note that this term is particularly important for low-frequency vibrations, as the right part of the second integral is largest in magnitude for low frequencies (see Figure 5).

If a phonon calculation is performed by using finite differences, there are several technical aspects one must consider. First, the size of the atomic displacements used must be tested carefully, as it is system dependent and also depends on the accuracy of the forces from the electronic-structure code. The displacements must be large enough not to cause numerical errors in the forces but small enough still to be in the harmonic regime. In our $ND_3$ case, displacements between 0.001 and 0.01 Å yielded consistent results with a force accuracy of $10^{-4}$ eV/Å, therefore, we have used 0.005 Å for all calculations. Second, a large enough cell has to be used so that the effect of one atomic displacement does not produce artifacts between periodic images. This was discussed for the X23 test set by Reilly and Tkatchenko[25] with the conclusion that for these systems, the cell should extend at least about 9–10 Å in each direction. However, this should be evaluated carefully for the studied system, especially for salts or molecular crystals involving heavier halogens. All of the calculations presented here were performed by using a 2×2×2 supercell. For numerical stability of the calculation, it is important to ensure that the reciprocal-space sampling in the supercell is exactly

  

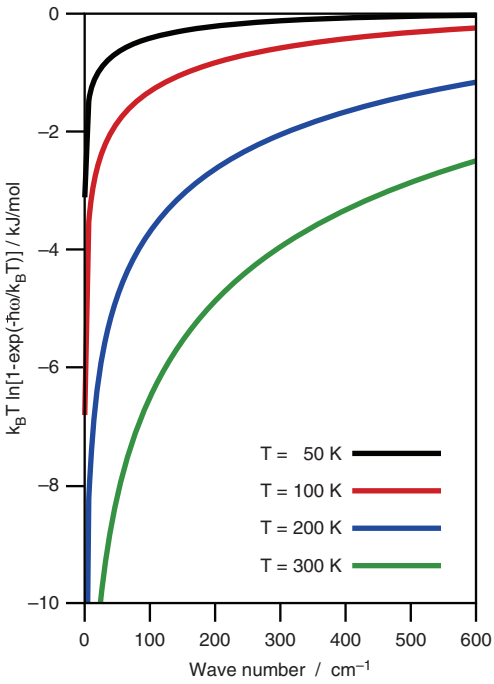


**FIGURE 5** | The temperature-dependent factor in the second integral of Eq. (10).

the same as in the optimized unit cell, i.e., if the unit cell was optimized with a $n \times n \times n$ $k$-point grid, a 2×2×2 supercell should have $\frac{n}{2} \times \frac{n}{2} \times \frac{n}{2}$ $k$ points. Furthermore, the pDOS has to be evaluated with a dense $k$-point grid in reciprocal space (or by calculating large supercells) in order to get accurate free energies. We have used the program phonopy,[112] which has interfaces to most of the popular periodic electronic-structure codes. Finally, the results have to be carefully analyzed for 'imaginary' frequencies. The appearance of an imaginary frequency at the Γ point indicates that the crystal is not in a local minimum of its PES and this will have a large impact on free energies and low-frequency phonon modes. Owing to the acoustic sum rule, the three acoustic modes have to be zero at the Γ point. However, small deviations are common due to the numeric nature of these calculations. Therefore, these three modes often have small imaginary frequencies, typically less than 1 $cm^{-1}$ in magnitude.

## Harmonic Helmholtz Free Energies

Using the harmonic Helmholtz free energies, the relative stability of polymorphs can be determined for desired thermodynamic conditions. It was shown by Marom et al.[105] and Rivera et al.[115] that zero-point energies can influence the calculated relative stabilities of glycine polymorphs. The aspirin crystal has two polymorphs with degenerated lattice energies, form I and form II, but form I is much more abundant experimentally. Considering only harmonic zero-point energies, the lattice-energy difference between the two polymorphs remains below 1 kJ/mol.[27] However, when considering $F_{\mathrm{vib}}^{\mathrm{HA}}$ at 300 K, form I becomes more stable by 2.6 kJ/mol when calculated with PBE+MBD. In the case of PBE+TS, form II is more stable by 0.7 kJ/mol. This shows the importance of both MBD interactions and Helmholtz free energies for the prediction of polymorph stabilities.

## Harmonic Vibrational Spectra

The pDOS provides information about all vibrational states within the molecular crystal, i.e., it contains not only modes accessible by IR and Raman spectroscopy (modes at the Γ point) but also out-of-phase phonon modes, which are long-range intermolecular modes. Figure 6(a) shows the calculated pDOS for the $ND_3$ crystal at the respective optimized geometry of PBE, PBE+TS, and PBE+MBD. The four peaks above 800 $cm^{-1}$ correspond to the internal vibrations of the ammonia molecules inside the crystal, i.e., inversions, angle bends, symmetric, and asymmetric stretching vibrations. The experimentally determined internal frequencies[116] for $ND_3$ are shown as gray lines in Figure 6(a). It can be seen that these frequencies are nicely captured by all three methods. In this frequency range, all the vibrations involve large energy changes, and therefore dispersion interactions play only a minor role for these vibrations. The peaks below 500 $cm^{-1}$ correspond to phonons (or lattice vibrations), i.e., vibrations involving intermolecular motion. Most of these low-frequency modes correspond to intermolecular translations and librations. If the molecules in a crystal have freely-rotating functional groups, like methyl groups, these low-energy intramolecular rotations can also occur in this frequency range. The low-frequency vibrations of $ND_3$ are shown in detail in Figure 6(b). It can be seen that there are qualitative differences, as well as shifts, in the peak positions of the pDOS between PBE and the vdW-inclusive methods. However, as our test system is a highly symmetric molecular crystal of a small, rigid molecule, the differences are small and stem mostly from differences in the optimized unit cells. For example, the unit-cell volume calculated with PBE is about 15% larger than with PBE+MBD, with the latter being closest to experiment.

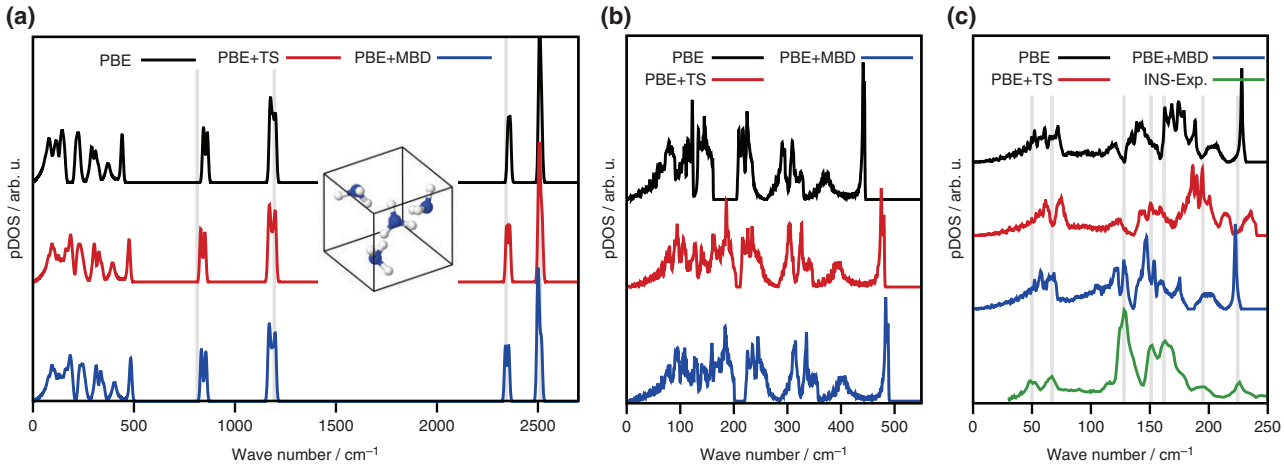


**FIGURE 6** | Full pDOS of $ND_3$ (a), the low-frequency region of the $ND_3$ pDOS (b), and the low-frequency region of the HMB pDOS (c). The gray lines in (a) show the location of the experimental internal modes as determined by Holt et al.,[116] and the gray lines in (c) mark the peak maxima of the experimental INS spectrum measured at 15 K by Ciezak et al.[117] HMB, hexamethylbenzene; INS, inelastic neutron scattering; $ND_3$, phase-I deutero ammonia; pDOS, phonon density of states.

In contrast, Figure 6(c) shows the low-frequency pDOS for a cubic HMB crystal calculated for the three methods at the experimental unit-cell volume. HMB has more flexibility than ammonia due to its methyl groups and the crystal is bound by dispersion interactions. In this case, we observe substantial differences in the pDOS between the different methods, even at the same volume. To understand how important these differences are, Figure 6(c) also shows an experimental inelastic neutron scattering (INS) spectrum, measured at 15 K.[117] As an INS spectrum does not represent a generalized pDOS, we cannot directly compare the intensities but be can directly compare the position of the peaks (see the gray lines). It can be seen that PBE+MBD reproduces the experimental peak positions very well, whereas the peaks of PBE and PBE+TS appear to be slightly shifted to higher frequencies. These spectra are compared at the experimental volume to allow for direct comparison in the absence of structural effects. The results are quite different if calculated at the respective minima of $E_{tot}$ for each method. In this case, the PBE structure has a significantly larger volume and therefore all peaks in the pDOS are shifted. Comparing different methods and experiment is therefore likely to be very sensitive to the temperature of the experiment and the unit cell used in calculating the spectra.

Although differences between the pDOS calculated with different methods can appear subtle, they can be very significant. Motta et al. recently calculated the pDOS of a durene crystal and found that including dispersion (using PBE+TS) was essential for getting good agreement with a low-temperature INS spectrum.[67] As noted above, the relative ordering of the two known polymorphs of aspirin changes significantly when calculating Helmholtz free energies with PBE+MBD or PBE+TS.[27] This can be traced to the pDOS calculated with the two methods. For PBE+TS, the two forms have comparable spectra but in the MBD case, a peak is found at about 30 $cm^{-1}$ for form I that is completely missing in the TS case and was also not found in form II. It is this difference in the pDOS of the two forms that leads to the changes in the calculated relative Helmholtz free energies and leads to PBE+MBD rationalizing the experimental observation of form I being more abundant.

In recent years, THz spectroscopy has emerged as very successful tool to detect drugs and explosives, as well as distinguish between different polymorphs of molecular crystals.[118,119] THz spectroscopy detects only vibrational modes at the Γ point, possesses the same selection rules as IR spectroscopy and is used to study only the low-frequency phonon modes, which are highly correlated with the packing arrangement of molecules inside a molecular crystal.

When we compare the intermolecular modes at the Γ point for our $ND_3$ example with experimental measurements, we observe, in general, deviations between 10 and 70 $cm^{-1}$. PBE always yields lower frequencies than the vdW-inclusive methods. The reason is mostly due to the overestimation of the unit-cell volume in the case of PBE. Furthermore, we are comparing calculated results without any consideration of thermal effects, while the experimental measurements correspond to temperatures between

  

18 and 61 K. Already at these temperatures, anharmonic effects due to thermal expansion and atomic motion lead to significant frequency shifts. Reilly et al.[120] extensively studied the lattice modes of ammonia and deutero ammonia by using the harmonic approximation as well as molecular-dynamics simulations. The observed difference between those methods amounts to 15–30 $cm^{-1}$ at 77 K.

The intensities of IR and THz spectra are proportional to the change of the dipole moment $\mu$

$$I_{IR} \propto \left(\frac{\partial \mu}{\partial Q}\right)^2 \quad (11)$$

where $Q$ is a normal-mode coordinate. Calculation of IR intensities is much more involved for periodic systems compared to molecules in vacuum because there is no unique definition of the dipole moment for periodic systems and therefore the calculation requires in principle a Berry-phase approach.[121] However, this option is not available in a large number of electronic-structure codes. The intensity of each mode can be calculated indirectly by calculating the difference between dipole moments of the unit cell calculated from atomic charges, e.g., Hirshfeld or Mulliken charges. This unit-cell dipole is then calculated for the ground state and for a geometry that is displaced along the normal-mode coordinate. Usually, this method is referred to as the *difference-dipole method*. Allis et al. have applied this approach for a variety of DFAs in order to calculate the THz spectrum of the explosive HMX.[122] This study shows that the THz modes highly depend on the DFA used. In recent years, vdW-inclusive DFT has been used to study the THz spectra of a number of molecular crystals including naproxen,[123] naphthalene,[124] durene,[124] enantiomers of ibuprofen,[2] isomers of benzenediols,[125] polymorphs of diclofenac acid,[126] and $\alpha$-D-glucose.[45] In general, vdW-inclusive DFT methods provide better THz spectra than traditional DFAs but major differences can be found between several vdW-inclusive methods. The best agreement between calculated THz spectra in the HA and experimental measurements is found at very low temperatures (<10 K), where anharmonic effects are likely to be minimized.

## What Is Missing in the Harmonic Approximation?

The harmonic approximation enables us to calculate free energies and obtain vibrational spectra. But what exactly are we missing in this approximation? As discussed before, we have omitted all higher-order terms in the Taylor expansion of the PES [see Eq. (7)]. So how valid is this approximation? To answer that question, we have taken two modes of $ND_3$ and calculated the energy with PBE+MBD for several displacements along the normal-mode coordinates (see Figure 7).

For a unitary displacement, the norm of the eigenvectors is equal to one. The mode in (a) shows an intermolecular translation and the mode in (b) corresponds to an internal wagging motion. It can be seen for (a) that the HA provides good results for small displacements from the equilibrium geometry but there are significant differences from the *exact* result at larger displacements. We can see from the energy scale in (a) that only a few kJ/mol are required to get into the anharmonic regime of that

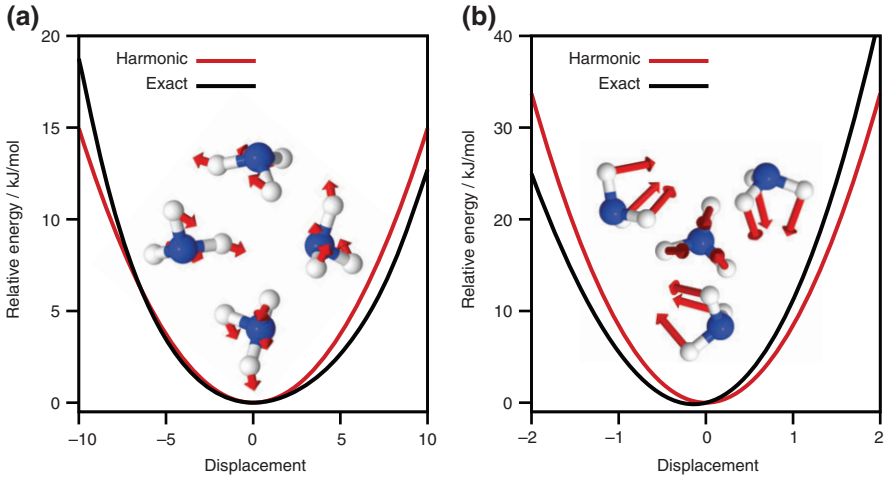


**FIGURE 7** | Harmonicity of two phonon modes in $ND_3$ calculated with PBE+MBD. The displacements are shown at a relative scale in which a displacement of 1 means that the norm of the eigenvectors is equal to one. MBD, many-body dispersion; $ND_3$, phase-I deutero ammonia.

  

phonon mode. This suggests that anharmonicity will be a serious issue for low-frequency phonon modes at high temperatures. Displacing along mode (b) requires much more energy compared to (a). In the case of (b), it can be clearly seen that the minimum of the harmonic curve does not correspond to the minimum of the *exact* curve. Considering these anharmonic effects would lead to a shift in the phonon-mode frequency.

Furthermore, the modes are described in the HA as independent oscillators, which means that there are no interactions or coupling between them. In a system at finite temperature, the motion of the atoms inside the crystal will certainly not be constrained to movements along normal-mode coordinates. Hence, in order to describe the atomic motion correctly, one would need at least a superposition of several normal modes. Another serious problem is that we have only approximated our PES around the minimum of the total energy $E_{tot}$. As a result, the pDOS corresponds to exactly this geometry and the free energy at finite temperatures also assumes that the structure of the system does not change at all with temperature. Therefore, it is not possible to observe or model phase transitions in the HA. One effect often neglected is the thermal expansion of molecular crystals. The volume of the unit cell will typically increase with increasing temperature. This will be discussed in detail in the next section. Finally, it is not possible to describe charge transport with the HA since phonon lifetimes and thermal conductivity are infinite.

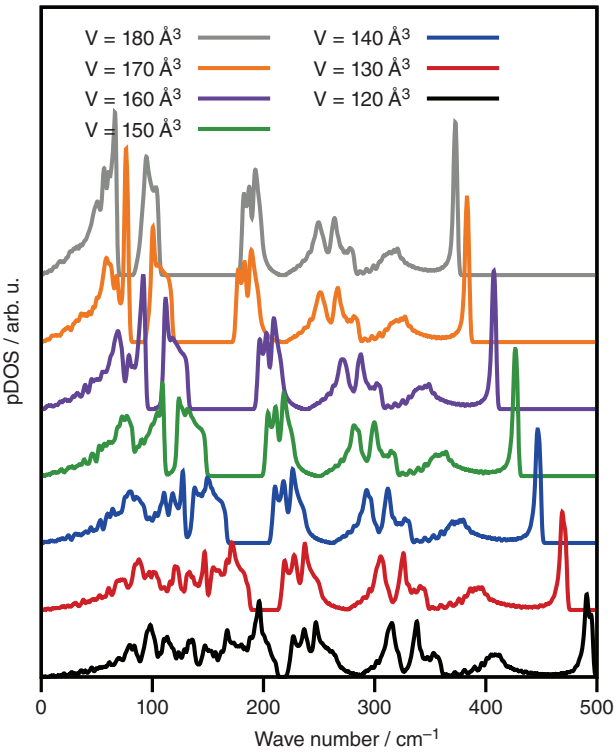


**FIGURE 8** | Phonon density of states of solid $ND_3$ calculated with PBE at several unit-cell volumes. $ND_3$, phase-I deutero ammonia.

## The Quasi-Harmonic Approximation

A straightforward way to improve upon the HA is the so-called quasi-harmonic approximation (QHA).[127] In this approximation, the HA is still applied but at several different unit-cell volumes. We start with the HA at the minimum of $E_{tot}$. Subsequently, the geometry of the unit cell is optimized for several fixed unit-cell volumes $V$ around the equilibrium unit-cell volume and the HA is applied to each of these structures. In the QHA, the free energy now depends explicitly on the unit-cell volume

$$F^{QHA}(T,V) = E_{tot}(V) + F^{HA}_{vib}(T,V) \qquad (12)$$

and therefore, the pDOS also depends on the cell volume. Figure 8 shows the dependence of the low-frequency pDOS on the unit-cell volume for the $ND_3$ crystal calculated at the PBE level of theory. It can be clearly seen that, in general, peaks shift to smaller frequencies with increasing volume and that the pDOS below 200 $cm^{-1}$ changes dramatically with increasing volume.

The result of applying the QHA is that we now know for several unit-cell volumes $V$, the harmonic free energy as a function of temperature $T$. Therefore, we can calculate the unit-cell volume corresponding to a specific temperature by fitting our data to an equation of state (EOS). The Murnaghan EOS[128] is often used for this purpose:

$$F^{QHA}(V) = F_0 + \frac{B_0 V}{B_0'}\left[\frac{(V_0/V)^{B_0'}}{B_0'-1}+1\right] - \frac{B_0 V_0}{B_0'-1} \qquad (13)$$

where $F_0$ is the equilibrium free energy for a certain temperature, $V_0$ is the corresponding equilibrium volume, $B_0$ is the bulk modulus at equilibrium volume $V_0$, and $B_0'$ is its pressure derivative.

## Thermal Expansion

Figure 9 shows the EOS fits for the model $ND_3$ crystal, while the resulting unit-cell volumes are

  

compared with the experimental data in Table 1. At 2 K, the unit-cell volume was measured experimentally as 128.6 Å$^3$. We can immediately see that a simple lattice optimization does not provide satisfactory results in terms of the unit-cell volume. The PBE functional overestimates $V$ by about 11% due to missing attractive interactions between the molecules and the two vdW-inclusive methods underestimate $V$ by about 4%. As discussed before, lattice optimizations do not take into account zero-point vibrations, which results in most cases in slightly too small unit-cell volumes for vdW-inclusive DFT.[25] The QHA includes zero-point vibrations and the DFA+vdW results agree at 2 K very well with experimental results; the error for PBE+TS and PBE+MBD amounts to 1.9 and 0.5%, respectively. Note, that PBE alone shows now an error of 17%, which illustrates how neglecting thermal and zero-point contributions can lead to spurious cancelation of some errors. It also reinforces the importance of dispersion interactions in modeling even a largely hydrogen-bonded system such as ammonia. Increasing the temperature to 180 K results in thermal expansion of about 5%.[129] PBE without dispersion now shows an error of about 22% in predicting the unit-cell volume, while PBE+TS and PBE+MBD provide a very reasonable description with errors being 2.5 and 1.5%, respectively. The PBE+MBD results agree consistently better with the experimental results than PBE+TS.

It is also possible to include pressure effects by simply adding the $pV$ term to $F^{\mathrm{QHA}}$, which then becomes $G^{\mathrm{QHA}}$.

$$G^{\mathrm{QHA}}(p,T,V) = E_{\mathrm{tot}}(V) + F_{\mathrm{vib}}^{\mathrm{HA}}(T,V) + pV \qquad (14)$$

At ambient conditions $pV$ is very small and is therefore neglected in our QHA calculations. If one wishes only to account for pressure effects without considering thermal effects, an external hydrostatic pressure can simply be added to the stress tensor. For example, Schatschneider et al. studied oligoacenes up to a pressure of 25 GPa using PBE+TS.[130] This hydrostatic external pressure also enables one to approximate thermal expansion. Describing the effect of $F_{\mathrm{vib}}^{\mathrm{HA}}(T,V)$ using just the $pV$ term leads to

$$p_{\mathrm{th}} = \frac{\partial F_{\mathrm{vib}}^{\mathrm{HA}}(T,V)}{\partial V} \qquad (15)$$

where $p_{\mathrm{th}}$ is a negative thermal pressure, which can be applied to the stress tensor during optimization to mimic thermal effects. In a very crude approximation, $p_{\mathrm{th}}$ can be obtained by finite differences using the free energies for a certain temperature of the optimized unit cell and a slightly larger or smaller unit cell. In order to demonstrate this, we have calculated the thermal pressure for the $ND_3$ model system for 180 K by considering only the optimized unit cell

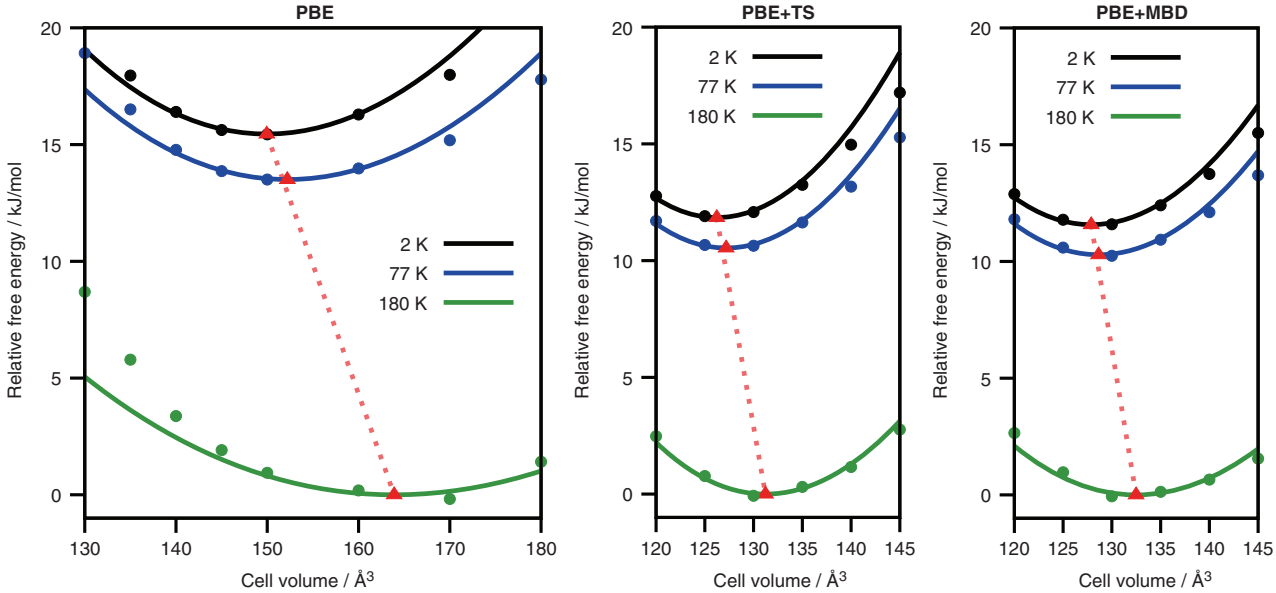


**FIGURE 9** | Quasi-harmonic approximation for solid $ND_3$ calculated with different methods at three different temperatures. The solid lines represent Murnaghan EOS fits and the red triangles mark the corresponding minima. EOS, equation of state; $ND_3$, phase-I deutero ammonia.

**TABLE 1** | Unit-Cell Volumes for $ND_3$ Phase I for Several Methods Calculated via Optimization (opt), Extracted from a Quasi-Harmonic Approximation ($n$ K) and Optimization under Thermal Pressure ($p_{th}$)

| Method | $V$(opt) [Å$^3$] | $V$(2 K) [Å$^3$] | $V$(77 K) [Å$^3$] | $V$(180 K) [Å$^3$] | $V(p_{th})$ [Å$^3$] | $p_{th}$ [GPa] |
|---|---|---|---|---|---|---|
| PBE | 142.6 | 149.9 | 152.2 | 163.9 | 162.6 | –0.52 |
| PBE+TS | 123.0 | 126.2 | 127.2 | 131.2 | 133.3 | –0.58 |
| PBE+MBD | 123.8 | 127.9 | 128.6 | 132.5 | 131.8 | –0.39 |
| Exp.[129] | — | 128.6 | 130.6 | 134.6 | — | — |

MBD, many-body dispersion; $ND_3$, phase-I deutero ammonia; TS, Tkatchenko–Scheffler.

and the closest available cell from the QHA, which has a larger volume than the optimized cell. This thermal pressure was then applied during a lattice relaxation. The obtained values for $p_{th}$ and the resulting volumes are presented in Table 1. It can be seen that the obtained volumes agree with the values from the QHA at 180 K within 2%. Using this thermal pressure approach, Otero-de-la-Roza and Johnson found that for the C21 dataset PBE+D2, PBE+TS, PBE+XDM, and vdW-DF2 yield mean absolute percentage deviations between 1.3 and 2.8% for cell lengths and between 0.1 and 0.3% for angles.[24]

Recently, Heit et al. studied the thermal expansion of crystalline carbon dioxide with the QHA using MP2.[40] Up to a temperature of 195 K, they underestimated the unit-cell volume by only about 2–3% compared to experiment. Erba et al. have recently reported the directional-dependent thermal expansion of the urea crystal studied within the QHA by using several density functional approximations and different dispersion corrections.[41]

The unit-cell volume for a specific temperature is determined by an interplay between the 0 K total energies and the vibrational free energies. A measure for the actual expansion of the crystal with temperature is the volumetric thermal expansion coefficient $\alpha_V$, which can be written as

$$\alpha_V = \frac{1}{V}\left(\frac{\partial V}{\partial T}\right)_p \tag{16}$$

The knowledge of $\alpha_V$ enables us to calculate also the heat capacity at constant pressure ($C_p$), which can be directly compared with experimental calorimetric measurements. $C_p$ is given by

$$C_p(T) = C_V(T) + \alpha_V(T)^2 B(T) V(T) T \tag{17}$$

where $B$ is the bulk modulus and $C_V$ can be calculated from

$$C_V = k_B \int d\omega g(\omega) \frac{(\hbar\omega/k_B T)^2 \exp(\hbar\omega/k_B T)}{[\exp(\hbar\omega/k_B T) - 1]^2} \tag{18}$$

Figure 10 shows the calculated values for $C_p$ and the linear thermal expansion coefficient $\alpha = \alpha_V/3$ for the $ND_3$ example compared with experimental values.[131] It can be seen that PBE overestimates $C_p$ at low temperatures and underestimates it at higher temperatures, whereas $\alpha$ is constantly overestimated by about 100%. In contrast, the vdW-inclusive methods underestimate $C_p$ and $\alpha$ by about 20%. The only exception is PBE+TS, which follows the experimental values at low temperature but starts underestimating $\alpha$ at about 100 K. This underestimation of thermal expansion is to be expected, since we are neglecting anharmonic effects due to internal atomic motion.

## Elastic Properties

Another type of response property that is highly temperature dependent is the elastic constants, which quantify a crystal's response to elastic deformation. The elastic constant matrix **C** of a molecular crystal can be obtained by a Taylor expansion around the equilibrium geometry:[132]

$$E(V, \varepsilon) = E_0 + V_0 \left( \sum_{i=1}^{6} \sigma_i \varepsilon_i + \frac{1}{2} \sum_{ij=1}^{6} C_{ij} \varepsilon_i \varepsilon_j \right) \tag{19}$$

where $\varepsilon$ is the strain applied to the unit cell and $\sigma$ is the corresponding stress of the unit cell. The elastic constants can then be approximated by the second-order derivatives of the energy with respect to the applied strain:

$$C_{ij} = \frac{1}{V_0} \frac{\partial^2 E}{\partial \varepsilon_i \partial \varepsilon_j} \tag{20}$$

Another approach to calculate the elastic constants is via the stress-strain relation

  

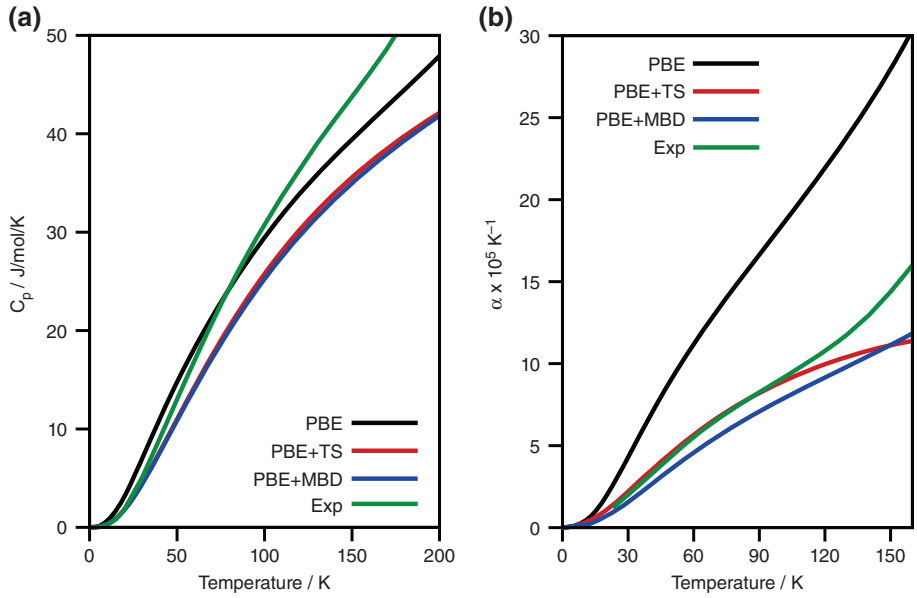


**FIGURE 10** | Heat capacity at constant pressure (a) and linear thermal expansion coefficient (b) of solid $ND_3$ obtained from the QHA compared to experimental values from Ref 131. $ND_3$, phase-I deutero ammonia; QHA, quasi-harmonic approximation.

$$\boldsymbol{\sigma} = \mathbf{C}\boldsymbol{\varepsilon} \tag{21}$$

where the elastic constant matrix is obtained by calculating the stress for several strained unit cells. Often, the elastic constants are calculated based on the equilibrium geometry and correspond therefore to 0 K. Thermal effects can also be included in a simple quasi-harmonic way by obtaining the unit-cell volume for the desired temperature from the QHA and calculating the elastic constants for this structure. We will illustrate this temperature dependence by using our $ND_3$ model crystal. Our example has a cubic unit cell and therefore possesses only three unique elastic constants: $C_{11}$, $C_{12}$, and $C_{44}$. The first two constants are related to volumetric elasticity and $C_{44}$ is related to shear deformation. The bulk modulus $B$ is an inverse measurement for the compressibility of the molecular crystal and can be calculated for a cubic crystal as

$$B = \frac{C_{11} + 2C_{12}}{3} \tag{22}$$

Calculated elastic constants for PBE, PBE+TS, and PBE+MBD are given in Table 2 and compared with experiment.

First, we compare the results obtained for the optimized geometries with the experimental values at 95 K. It can be seen that PBE underestimates the bulk modulus and all elastic constants while both vdW-inclusive methods overestimate the experimental values. Comparing the results obtained at the estimated unit-cell volumes at 194 K with the experimental results at 194 K, we can see that all of the elastic constants decrease with increasing temperature (and hence volume). The PBE bulk modulus is now almost three times smaller than the experimental value, while the vdW-inclusive methods agree very well with experiment. The deviation in the bulk modulus is 1.0 GPa for PBE+TS and only 0.1 GPa for PBE+MBD.

Another important elastic property of a crystal is the Young's modulus, which describes the tendency of deformation along an axis and can also be calculated directly from the elastic constants. Figure 11 shows spherical polar plots of the Young's modulus of ammonia. The plot for PBE is very isotropic, while PBE+MBD is more anisotropic. If we compare the plots of the optimized geometries with the experimental plot, one might think that PBE is describing the Young's modulus better than PBE+MBD, but when we compare the values for 194 K, we can immediately see that vdW interactions have a large influence on elastic properties. We can also measure the anisotropy of the elastic constants with the so-called anisotropy factor $A$, which for cubic crystals is given by

$$A = \frac{2C_{44}}{C_{11} - C_{12}} \tag{23}$$

It can be seen that PBE+MBD shows the largest anisotropy among the theoretical values, but stills

  

**TABLE 2** | Elastic Constants, Bulk Modulus, and Anisotropy Ratio for Solid $ND_3$ Calculated at the Minima of $E_{tot}$ (opt) and at Volumes Corresponding to 194 K According to Respective QHAs, Compared to Experimental Values

| Method | $C_{11}$ [GPa] | $C_{12}$ [GPa] | $C_{44}$ [GPa] | $B$ [GPa] | A |
|---|---|---|---|---|---|
| PBE(opt) | 9.8±0.3 | 3.7±0.1 | 4.6±0.1 | 5.7 | 1.5 |
| PBE+TS(opt) | 15.6±0.4 | 6.8±0.3 | 8.3±0.1 | 9.8 | 1.9 |
| PBE+MBD(opt) | 15.6±0.2 | 6.4±0.1 | 8.7±0.1 | 9.5 | 1.9 |
| PBE(194 K) | 3.5±0.2 | 1.6±0.1 | 1.3±0.1 | 2.3 | 1.4 |
| PBE+TS(194 K) | 9.8±0.3 | 3.7±0.2 | 5.0±0.1 | 5.8 | 1.6 |
| PBE+MBD(194 K) | 11.0±0.3 | 4.6±0.2 | 5.8±0.1 | 6.7 | 1.8 |
| Exp(95 K)[134] | 10.0±0.5 | 5.6±1.0 | 5.6±0.4 | 7.1 | 2.5 |
| Exp(194 K)[135] | 9.5±0.8 | 5.5±0.9 | 4.9±0.4 | 6.8 | 2.4 |

MBD, many-body dispersion; $ND_3$, phase-I deutero ammonia; QHA, quasi-harmonic approximation; TS, Tkatchenko–Scheffler.

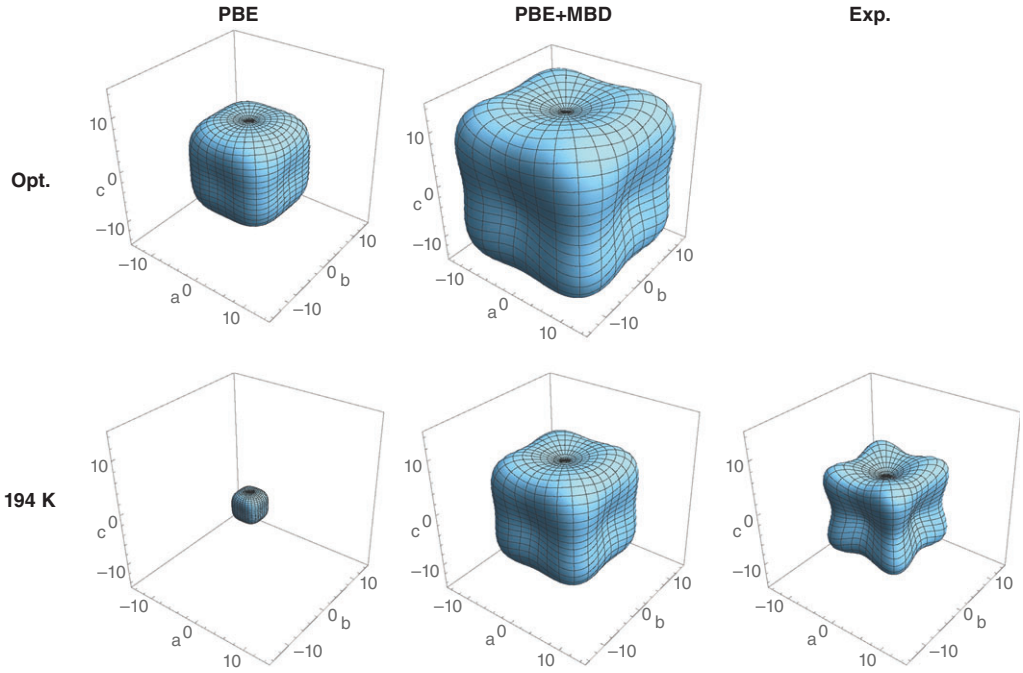


**FIGURE 11** | Spherical plots of the Young's modulus of $ND_3$ (in GPa) obtained at the minima of $E_{tot}$ (opt) and at volumes corresponding to 194 K from the QHA for PBE and PBE+MBD, as well as experimental values at 194 K of Ref 135. MBD, many-body dispersion; $ND_3$, phase-I deutero ammonia; QHA, quasi-harmonic approximation.

underestimates the degree of anisotropy compared to experimental measurements, likely due to the lack of anharmonicity in calculating the elastic constants.

The use of DFAs for studying mechanical properties has grown in recent years. The elastic properties of urea have been studied by Erba et al. in a quasi-harmonic fashion yielding encouraging results for PBE, PBE0, and B3LYP when paired with the D3 dispersion correction.[41] The mechanical properties of the two aspirin polymorphs have also been studied using PBE+TS and PBE+MBD.[27] Despite their near degenerate lattice energies and a free-energy difference of 2.6 kJ/mol, the two forms show remarkably different elastic properties. As in the case of ammonia, PBE+MBD also yields more anisotropic elastic response for the two polymorphs of aspirin and smaller elastic constants, agreeing better with experimental values.

## CONCLUSIONS

The prediction and modeling of molecular crystals from first principles has evolved considerably in recent years. With the development of accurate vdW-inclusive DFT methods, in particular, first-principles

  

methods can now be applied to realistic molecular crystals, leading to new insights and understanding of structure, stabilities, polymorphism, and response properties such as phonons and elastic moduli. This ability of first-principles methods to model these properties in an accurate, balanced, and transferable fashion will make methods such as vdW-inclusive DFT central tools for predicting and engineering molecular crystals in future. High-level first-principles methods such as MP2 and beyond can already be applied to several molecular crystals and encouraging progress is being made to enable the applications for realistic systems in the future.[71] Also, the utilization of symmetry-adapted perturbation theory for periodic systems will enable new insights into the nature of intermolecular interactions in molecular crystals.[86]

The current state of the art in first-principles methods enables us to calculate lattice energies with a accuracy better than 4.2 kJ/mol. Key to achieving this accuracy is to go beyond a pairwise model of dispersion and include nonadditive many-body contributions, for example, by using the MBD method.[22,91] Truly predicting and understanding phenomena such as polymorphism requires greater accuracy still, with a number of studies of a range of systems having shown the importance of thermal and pressure contributions to the relative stabilities of polymorphs.[133]

Another key aspect of modeling molecular crystals is in understanding that all of their properties (including their structure) can be highly temperature dependent. Many first-principles studies of molecular crystals treat them in the harmonic limit. While this can give powerful insights, the harmonic approximation neglects anharmonic effects due to the expansion of the unit cell and thermal motion. Omitting these effects when calculating derived properties and quantities such as low-frequency vibrational spectra (THz spectra) and elastic constants, can lead to large deviations between experiment and theory, as we have shown using our model system of phase-I deutero ammonia. An efficient way of approximating anharmonic contributions with first-principles methods is the quasi-harmonic approximation, which captures the majority of the thermal expansion.

Perhaps one of the most important directions in first-principles modeling of molecular crystals is the development of accurate force fields derived from first-principles data. Recent results already show encouraging accuracy for molecular crystals.[102] Such force fields would enable the types of molecular-dynamics simulations and multiscale models needed to fully understand the thermodynamics and kinetics of molecular crystals as a function of temperature and other variables. At the same time, fully first-principles methods can be used to determine the underlying electronic energies and key response properties accurately, providing a full picture of the formation, stability, and properties of molecular crystals.

## ACKNOWLEDGMENT

J.H. and A.T. acknowledge the support from the Deutsche Forschungsgemeinschaft under the program DFG-SPP 1807.

## REFERENCES

1. Bauer J, Spanton S, Henry R, Quick J, Dziki W, Porter W, Morris J. Ritonavir: an extraordinary example of conformational polymorphism. *Pharm Res* 2001, 18:859–866.
2. King MD, Buchanan WD, Korter TM. Understanding the terahertz spectra of crystalline pharmaceuticals: terahertz spectroscopy and solid-state density functional theory study of (S)-(+)-ibuprofen and (RS)-ibuprofen. *J Pharm Sci* 2011, 100:1116–1129.
3. Davies AG, Burnett AD, Fan W, Linfield EH, Cunningham JE. Terahertz spectroscopy of explosives and drugs. *Mater Today* 2008, 11:18–26.
4. Dimitrakopoulos CD, Malenfant PRL. Organic thin film transistors for large area electronics. *Adv Mater* 2002, 14:99–117.
5. Anthony JE. Functionalized acenes and heteroacenes for organic electronics. *Chem Rev* 2006, 106:5028–5048.
6. Coropceanu V, Cornil J, da Silva Filho DA, Olivier Y, Silbey R, Brédas J-L. Charge transport in organic semiconductors. *Chem Rev* 2007, 107:926–952.
7. Anthony JE. The larger acenes: versatile organic semiconductors. *Angew Chem Int Ed* 2008, 47:452–483.
8. Kaupp G. Solid-state reactions, dynamics in molecular crystals. *Curr Opin Solid State Mater Sci* 2002, 6:131–138.
9. Datta S, Grant DJW. Crystal structures of drugs: advances in determination, prediction and engineering. *Nat Rev Drug Discov* 2004, 3:42–57.

  

10. Desiraju GR. Crystal engineering: from molecule to crystal. *J Am Chem Soc* 2013, 135:9952–9967.
11. Bartlett RJ. Coupled-cluster theory and its equation-of-motion extensions. *Wiley Interdiscip Rev Comput Mol Sci* 2012, 2:126–138.
12. Dubecký M, Jurečka P, Derian R, Hobza P, Otyepka M, Mitas L. Quantum Monte Carlo methods describe noncovalent interactions with subchemical accuracy. *J Chem Theory Comput* 2013, 9:4287–4292.
13. Jurečka P, Šponer J, Černý J, Hobza P. Benchmark database of accurate (MP2 and CCSD(T) complete basis set limit) interaction energies of small model complexes, DNA base pairs, and amino acid pairs. *Phys Chem Chem Phys* 2006, 8:1985–1993.
14. Řezáč J, Riley KE, Hobza P. S66: a well-balanced database of benchmark interaction energies relevant to biomolecular structures. *J Chem Theory Comput* 2011, 7:2427–2438.
15. Ambrosetti A, Alfè D, DiStasio RA Jr, Tkatchenko A. Hard numbers for large molecules: toward exact energetics for supramolecular systems. *J Phys Chem Lett* 2014, 5:849–855.
16. Grimme S. Semiempirical GGA-type density functional constructed with a long-range dispersion correction. *J Comput Chem* 2006, 27:1787–1799.
17. Grimme S, Antony J, Ehrlich S, Krieg H. A consistent and accurate *ab initio* parametrization of density functional dispersion correction (DFT-D) for the 94 elements H-Pu. *J Chem Phys* 2010, 132:154104.
18. Becke AD, Johnson ER. Exchange-hole dipole moment and the dispersion interaction revisited. *J Chem Phys* 2007, 127:154108.
19. Tkatchenko A, Scheffler M. Accurate molecular van der Waals interactions from ground-state electron density and free-atom reference data. *Phys Rev Lett* 2009, 102:073005.
20. Tkatchenko A, DiStasio RA Jr, Car R, Scheffler M. Accurate and efficient method for many-body van der Waals interactions. *Phys Rev Lett* 2012, 108:236402.
21. Grimme S. Density functional theory with London dispersion corrections. *Wiley Interdiscip Rev Comput Mol Sci* 2011, 1:211–228.
22. Grimme S, Hansen A, Brandenburg JG, Bannwarth C. Dispersion-corrected mean-field electronic structure methods. *Chem Rev* 2016, 116:5105–5154.
23. Boese AD. Density functional theory and hydrogen bonds: are we there yet? *ChemPhysChem* 2015, 16:978–985.
24. Otero-de-la-Roza A, Johnson ER. A benchmark for non-covalent interactions in solids. *J Chem Phys* 2012, 137:054103.
25. Reilly AM, Tkatchenko A. Understanding the role of vibrations, exact exchange, and many-body van der Waals interactions in the cohesive properties of molecular crystals. *J Chem Phys* 2013, 139:024705.
26. Cruz-Cabeza AJ, Reutzel-Edens SM, Bernstein J. Facts and fictions about polymorphism. *Chem Soc Rev* 2015, 44:8619–8635.
27. Reilly AM, Tkatchenko A. Role of dispersion interactions in the polymorphism and entropic stabilization of the aspirin crystal. *Phys Rev Lett* 2014, 113:055701.
28. Nyman J, Day GM. Static and lattice vibrational energy differences between polymorphs. *CrystEngComm* 2015, 17:5154–5165.
29. Hylton RK, Tizzard GJ, Threlfall TL, Ellis AL, Coles SJ, Seaton CC, Schulze E, Lorenz H, Seidel-Morgenstern A, Stein M, et al. Are the crystal structures of enantiopure and racemic mandelic acids determined by kinetics or thermodynamics? *J Am Chem Soc* 2015, 137:11095–11104.
30. Price SL. Why don't we find more polymorphs? *Acta Crystallogr Sect B Struct Sci Cryst Eng Mater* 2013, 69:313–328.
31. Szabo A, Ostlund NS. *Modern Quantum Chemistry: Introduction to Advanced Electronic Structure Theory*. Dover Books on Chemistry. Mineola, NY: Dover Publications; 1989.
32. Cremer D. From configuration interaction to coupled cluster theory: the quadratic configuration interaction approach. *Wiley Interdiscip Rev Comput Mol Sci* 2013, 3:482–503.
33. Frenkel D, Smit B. *Understanding Molecular Simulation: From Algorithms to Applications*. 2nd ed. San Diego: Academic Press; 2002.
34. Deij MA, ter Horst JH, Meekes H, Jansens P, Vlieg E. Polymorph formation studied by 3D nucleation simulations. Application to a yellow isoxazolone dye, paracetamol, and L-glutamic acid. *J Phys Chem B* 2007, 111:1523–1530.
35. Boerrigter SXM, Josten GPH, van de Streek J, Hollander FFA, Los J, Cuppen HM, Bennema P, Meekes H. MONTY: Monte Carlo crystal growth on any crystal structure in any crystallographic orientation; application to fats. *J Phys Chem A* 2004, 108:5894–5902.
36. Piana S, Reyhani M, Gale JD. Simulating micrometre-scale crystal growth from solution. *Nature* 2005, 438:70–73.
37. Price SL. Predicting crystal structures of organic compounds. *Chem Soc Rev* 2014, 43:2098–2111.
38. Salvalaglio M, Vetter T, Giberti F, Mazzotti M, Parrinello M. Uncovering molecular details of urea crystal growth in the presence of additives. *J Am Chem Soc* 2012, 134:17221–17233.
39. Anwar J, Zahn D. Uncovering molecular processes in crystal nucleation and growth by using molecular simulation. *Angew Chem Int Ed* 2011, 50:1996–2013.
40. Heit YN, Nanda KD, Beran GJO. Predicting finite temperature properties of crystalline carbon dioxide


  

from first principles with quantitative accuracy. *Chem Sci* 2016, 7:246–255.

41. Erba A, Maul J, Civalleri B. Thermal properties of molecular crystals through dispersion-corrected quasi-harmonic *ab initio* calculations: the case of urea. *Chem Commun* 2016, 52:1820–1823.
42. Monserrat B, Drummond ND, Needs RJ. Anharmonic vibrational properties in periodic systems: energy, electron-phonon coupling, and stress. *Phys Rev B* 2013, 87:144302.
43. Drummond ND, Monserrat B, Lloyd-Williams JH, Ríos PL, Pickard CJ, Needs RJ. Quantum Monte Carlo study of the phase diagram of solid molecular hydrogen at extreme pressures. *Nat Commun* 2015, 6:7794.
44. Engel EA, Monserrat B, Needs RJ. Anharmonic nuclear motion and the relative stability of hexagonal and cubic ice. *Phys Rev X* 2015, 5:021033.
45. Takahashi M, Ishikawa Y. Terahertz vibrations of crystalline α-D-glucose and the spectral change in mutual transitions between the anhydride and monohydrate. *Chem Phys Lett* 2015, 642:29–34.
46. Adhikari K, Flurchick KM, Valenzano L. Volumetric influence on the mechanical behavior of organic solids: the case of aspirin and paracetamol addressed via dispersion corrected DFT. *Chem Phys Lett* 2015, 630:44–50.
47. Reilly AM, Cooper RI, Adjiman CS, Bhattacharya S, Boese AD, Brandenburg JG, Bygrave PJ, Bylsma R, Campbell JE, Car R, et al. Report on the sixth blind test of organic crystal structure prediction methods. *Acta Crystallogr Sect B Struct Sci Cryst Eng Mater* 2016, 72:439–459.
48. Schatschneider B, Liang J-J, Jezowski S, Tkatchenko A. Phase transition between cubic and monoclinic polymorphs of the tetracyanoethylene crystal: the role of temperature and kinetics. *CrystEngComm* 2012, 14:4656–4663.
49. Stone A. *The Theory of Intermolecular Forces*. 2nd ed. Oxford: Oxford Press; 2013.
50. Jeziorski B, Moszynski R, Szalewicz K. Perturbation theory approach to intermolecular potential energy surfaces of van der Waals complexes. *Chem Rev* 1994, 94:1887–1930.
51. Ferri N, DiStasio RA Jr, Ambrosetti A, Car R, Tkatchenko A. Electronic properties of molecules and surfaces with a self-consistent interatomic van der Waals density functional. *Phys Rev Lett* 2015, 114:176802.
52. Dobson JF, Gould T. Calculation of dispersion energies. *J Phys Condens Matter* 2012, 24:073201.
53. Jeffrey GA. *An Introduction to Hydrogen Bonding*. New York: Oxford University Press; 1997.
54. Hoja J, Sax AF, Szalewicz K. Is electrostatics sufficient to describe hydrogen-bonding interactions? *Chem Eur J* 2014, 20:2292–2300.
55. Stone AJ. Are halogen bonded structures electrostatically driven? *J Am Chem Soc* 2013, 135:7005–7009.
56. Riley KE, Hobza P. The relative roles of electrostatics and dispersion in the stabilization of halogen bonds. *Phys Chem Chem Phys* 2013, 15:17742–17751.
57. Szalewicz K. Symmetry-adapted perturbation theory of intermolecular forces. *Wiley Interdiscip Rev Comput Mol Sci* 2012, 2:254–272.
58. Jansen G. Symmetry-adapted perturbation theory based on density functional theory for noncovalent interactions. *Wiley Interdiscip Rev Comput Mol Sci* 2014, 4:127–144.
59. Lommerse JPM, Motherwell WDS, Ammon HL, Dunitz JD, Gavezzotti A, Hofmann DWM, Leusen FJJ, Mooij WTM, Price SL, Schweizer B, et al. A test of crystal structure prediction of small organic molecules. *Acta Crystallogr Sect B Struct Sci* 2000, 56:697–714.
60. Motherwell WDS, Ammon HL, Dunitz JD, Dzyabchenko A, Erk P, Gavezzotti A, Hofmann DWM, Leusen FJJ, Lommerse JPM, Mooij WTM, et al. Crystal structure prediction of small organic molecules: a second blind test. *Acta Crystallogr Sect B Struct Sci* 2002, 58:647–661.
61. Day GM, Motherwell WDS, Ammon HL, Boerrigter SXM, Della Valle RG, Venuti E, Dzyabchenko A, Dunitz JD, Schweizer B, van Eijck BP, et al. A third blind test of crystal structure prediction. *Acta Crystallogr Sect B Struct Sci* 2005, 61:511–527.
62. Day GM, Cooper TG, Cruz-Cabeza AJ, Hejczyk KE, Ammon HL, Boerrigter SXM, Tan JS, Della Valle RG, Venuti E, Jose J, et al. Significant progress in predicting the crystal structures of small organic molecules a report on the fourth blind test. *Acta Crystallogr Sect B Struct Sci* 2009, 65:107–125.
63. Bardwell DA, Adjiman CS, Arnautova YA, Bartashevich E, Boerrigter SXM, Braun DE, Cruz-Cabeza AJ, Day GM, Della Valle RG, Desiraju GR, et al. Towards crystal structure prediction of complex organic compounds a report on the fifth blind test. *Acta Crystallogr Sect B Struct Sci* 2011, 67:535–551.
64. Schmidt MU, Brüning J, Glinnemann J, Hützler MW, Mörschel P, Ivashevskaya SN, van de Streek J, Braga D, Maini L, Chierotti MR, et al. The thermodynamically stable form of solid barbituric acid: the enol tautomer. *Angew Chem Int Ed* 2011, 50:7924–7926.
65. Thompson HPG, Day GM. Which conformations make stable crystal structures? Mapping crystalline molecular geometries to the conformational energy landscape. *Chem Sci* 2014, 5:3173–3182.
66. Cruz-Cabeza AJ, Bernstein J. Conformational polymorphism. *Chem Rev* 2014, 114:2170–2191.

  

67. Motta C, Sanvito S. Charge transport properties of durene crystals from first-principles. *J Chem Theory Comput* 2014, 10:4624–4632.
68. Pickard CJ, Mauri F. All-electron magnetic response with pseudopotentials: NMR chemical shifts. *Phys Rev B* 2001, 63:245101.
69. Charpentier T. The PAW/GIPAW approach for computing NMR parameters: a new dimension added to NMR study of solids. *Solid State Nucl Magn Reson* 2011, 40:1–20.
70. Hartman JD, Monaco S, Schatschneider B, Beran GJO. Fragment-based $^{13}C$ nuclear magnetic resonance chemical shift predictions in molecular crystals: an alternative to planewave methods. *J Chem Phys* 2015, 143:102809.
71. Beran GJO. Modeling polymorphic molecular crystals with electronic structure theory. *Chem Rev* 2016, 116:5567–5613.
72. Neumann MA. Tailor-made force fields for crystal-structure prediction. *J Phys Chem B* 2008, 112:9810–9829.
73. Stone AJ. Distributed multipole analysis: stability for large basis sets. *J Chem Theory Comput* 2005, 1:1128–1132.
74. Brandenburg JG, Grimme S. Accurate modeling of organic molecular crystals by dispersion-corrected density functional tight binding (DFTB). *J Phys Chem Lett* 2014, 5:1785–1789.
75. Stöhr M, Michelitsch GS, Tully JC, Reuter K, Maurer RJ. Communication: charge-population based dispersion interactions for molecules and materials. *J Chem Phys* 2016, 144:151101.
76. Lee K, Murray ÉD, Kong L, Lundqvist BI, Langreth DC. Higher-accuracy van der Waals density functional. *Phys Rev B* 2010, 82:081101.
77. Maschio L, Usvyat D, Schütz M, Civalleri B. Periodic local Møller– Plesset second order perturbation theory method applied to molecular crystals: study of solid $NH_3$ and $CO_2$ using extended basis sets. *J Chem Phys* 2010, 132:134706.
78. Erba A, Pisani C, Casassa S, Maschio L, Schütz M, Usvyat D. MP2 versus density-functional theory study of the Compton profiles of crystalline urea. *Phys Rev B* 2010, 81:165108.
79. Grüneis A, Marsman M, Kresse G. Second-order Møller-Plesset perturbation theory applied to extended systems II. Structural and energetic properties. *J Chem Phys* 2010, 133:074107.
80. Hongo K, Watson MA, Sánchez-Carrera RS, Iitaka T, Aspuru-Guzik A. Failure of conventional density functionals for the prediction of molecular crystal polymorphism: a Quantum Monte Carlo study. *J Phys Chem Lett* 2010, 1:1789–1794.
81. Hongo K, Watson MA, Iitaka T, Aspuru-Guzik A, Maezono R. Diffusion Monte Carlo study of paradiiodobenzene polymorphism revisited. *J Chem Theory Comput* 2015, 11: 907–917.
82. Yang J, Hu W, Usvyat D, Matthews D, Schütz M, Chan GK-L. *Ab initio* determination of the crystalline benzene lattice energy to sub-kilojoule/mole accuracy. *Science* 2014, 345:640–643.
83. Beran GJO. A new era for *ab initio* molecular crystal lattice energy prediction. *Angew Chem Int Ed* 2015, 54:396–398.
84. Wen S, Nanda K, Huang Y, Beran GJO. Practical quantum mechanics-based fragment methods for predicting molecular crystal properties. *Phys Chem Chem Phys* 2012, 14:7578–7590.
85. Beran GJO, Nanda K. Predicting organic crystal lattice energies with chemical accuracy. *J Phys Chem Lett* 2010, 1:3480–3487.
86. Szalewicz K. Determination of structure and properties of molecular crystals from first principles. *Acc Chem Res* 2014, 47:3266–3274.
87. Grimme S, Ehrlich S, Goerigk L. Effect of the damping function in dispersion corrected density functional theory. *J Comp Chem* 2011, 32:1456–1465.
88. Blood-Forsythe MA, Markovich T, DiStasio RA Jr, Car R, Aspuru-Guzik A. Analytical nuclear gradients for the range-separated many-body dispersion model of noncovalent interactions. *Chem Sci* 2016, 7:1712–1728.
89. Becke AD, Johnson ER. Exchange-hole dipole moment and the dispersion interaction: high-order dispersion coefficients. *J Chem Phys* 2006, 124:014104.
90. Johnson ER. Dependence of dispersion coefficients on atomic environment. *J Chem Phys* 2011, 135:234109.
91. Reilly AM, Tkatchenko A. van der Waals dispersion interactions in molecular materials: beyond pairwise additivity. *Chem Sci* 2015, 6:3289–3301.
92. Ambrosetti A, Reilly AM, DiStasio RA Jr, Tkatchenko A. Long-range correlation energy calculated from coupled atomic response functions. *J Chem Phys* 2014, 140:18A508.
93. Tkatchenko A. Current understanding of van der Waals effects in realistic materials. *Adv Func Mat* 2015, 25:2054–2061.
94. Ambrosetti A, Ferri N, DiStasio RA Jr, Tkatchenko A. Wavelike charge density fluctuations and van der Waals interactions at the nanoscale. *Science* 2016, 351:1171–1176.
95. Gobre VV, Tkatchenko A. Scaling laws for van der Waals interactions in nanostructured materials. *Nat Commun* 2013, 4:2341.
96. Nanda KD, Beran GJO. Prediction of organic molecular crystal geometries from MP2-level fragment quantum mechanical/molecular mechanical calculations. *J Chem Phys* 2012, 137:174106.


  

97. Wen S, Beran GJO. Accurate molecular crystal lattice energies from a fragment QM/MM approach with on-the-fly *ab initio* force field parametrization. *J Chem Theory Comput* 2011, 7:3733–3742.
98. Maschio L, Civalleri B, Ugliengo P, Gavezzotti A. Intermolecular interaction energies in molecular crystals: comparison and agreement of localized Møller–Plesset 2, dispersion-corrected density functional, and classical empirical two-body calculations. *J Phys Chem A* 2011, 115:11179–11186.
99. Civalleri B, Zicovich-Wilson CM, Valenzano L, Ugliengo P. B3LYP augmented with an empirical dispersion term (B3LYP-D*) as applied to molecular crystals. *CrystEngComm* 2008, 10:405–410.
100. Perdew JP, Burke K, Ernzerhof M. Generalized gradient approximation made simple. *Phys Rev Let* 1996, 77:3865–3868.
101. Moellmann J, Grimme S. DFT-D3 study of some molecular crystals. *J Phys Chem C* 2014, 118:7615–7621.
102. Nyman J, Pundyke OS, Day GM. Accurate force fields and methods for modelling organic molecular crystals at finite temperatures. *Phys Chem Chem Phys* 2016, 18:15828–15837.
103. Bradley RS, Cotson S. 347. The vapour pressure and lattice energy of hydrogen-bonded crystals. Part II. ∝- and β-anhydrous oxalic acid and tetragonal pentaerythritol. *J Chem Soc* 1953:1684–1688.
104. de Wit HGM, Bouwstra JA, Blok JG, de Kruif CG. Vapor pressures and lattice energies of oxalic acid, mesotartaric acid, phloroglucinol, myoinositol, and their hydrates. *J Chem Phys* 1983, 78:1470–1475.
105. Marom N, DiStasio RA Jr, Atalla V, Levchenko S, Reilly AM, Chelikowsky JR, Leiserowitz L, Tkatchenko A. Many-body dispersion interactions in molecular crystal polymorphism. *Angew Chem Int Ed* 2013, 52:6629–6632.
106. Schatschneider B, Monaco S, Liang J-J, Tkatchenko A. High-throughput investigation of the geometry and electronic structures of gas-phase and crystalline polycyclic aromatic hydrocarbons. *J Phys Chem C* 2014, 118:19964–19974.
107. Mermin ND. Thermal properties of the inhomogeneous electron gas. *Phys Rev* 1965, 137:A1441–A1443.
108. Blum V, Gehrke R, Hanke F, Havu P, Havu V, Ren X, Reuter K, Scheffler M. *Ab initio* molecular simulations with numeric atom-centered orbitals. *Comput Phys Commun* 2009, 180:2175–2196.
109. Marek A, Blum V, Johanni R, Havu V, Lang B, Auckenthaler T, Heinecke A, Bungartz H-J, Lederer H. The ELPA library: scalable parallel eigenvalue solutions for electronic structure theory and computational science. *J Phys Condens Matter* 2014, 26:213201.
110. Auckenthaler T, Blum V, Bungartz H-J, Huckle T, Johanni R, Krämer L, Lang B, Lederer H, Willems P. Parallel solution of partial symmetric eigenvalue problems from electronic structure calculations. *Parallel Comput* 2011, 37:783–794.
111. Havu V, Blum V, Havu P, Scheffler M. Efficient O(N) integration for all-electron electronic structure calculation using numeric basis functions. *J Comput Phys* 2009, 228:8367–8379.
112. Togo A, Tanaka I. First principles phonon calculations in materials science. *Scr Mater* 2015, 108:1–5.
113. Ashcroft NW, Mermin ND. *Solid State Physics*. Philadelphia, PA: Saunders College; 1976.
114. Baroni S, de Gironcoli S, Dal Corso A, Giannozzi P. Phonons and related crystal properties from density-functional perturbation theory. *Rev Mod Phys* 2001, 73:515–562.
115. Rivera SA, Allis DG, Hudson BS. Importance of vibrational zero-point energy contribution to the relative polymorph energies of hydrogen-bonded species. *Cryst Growth Des* 2008, 8:3905–3907.
116. Holt JS, Sadoskas D, Pursell CJ. Infrared spectroscopy of the solid phases of ammonia. *J Chem Phys* 2004, 120:7153–7157.
117. Ciezak JA, Hudson BS. Vibrational analysis of the inelastic neutron scattering spectrum of tetracyanoethylene–hexamethylbenzene by electronic structure calculations. *J Mol Struct (THEOCHEM)* 2005, 755:195–202.
118. Takahashi M. Terahertz vibrations and hydrogen-bonded networks in crystals. *Crystals* 2014, 4:74–103.
119. McIntosh AI, Yang B, Goldup SM, Watkinson M, Donnan RS. Terahertz spectroscopy: a powerful new tool for the chemical sciences? *Chem Soc Rev* 2012, 41:2072–2082.
120. Reilly AM, Middlemiss DS, Siddick MM, Wann DA, Ackland GJ, Wilson CC, Rankin DWH, Morrison CA. The phonon spectrum of phase-I ammonia: reassignment of lattice mode symmetries from combined molecular and lattice dynamics calculations. *J Phys Chem A* 2008, 112:1322–1329.
121. Spaldin NA. A beginner's guide to the modern theory of polarization. *J Solid State Chem* 2012, 195:2–10.
122. Allis DG, Prokhorova DA, Korter TM. Solid-state modeling of the terahertz spectrum of the high explosive HMX. *J Phys Chem A* 2006, 110:1951–1959.
123. King MD, Buchanan WD, Korter TM. Application of London-type dispersion corrections to the solid-state density functional theory simulation of the terahertz spectra of crystalline pharmaceuticals. *Phys Chem Chem Phys* 2011, 13:4250–4259.
124. King MD, Korter TM. Modified corrections for London forces in solid-state density functional theory calculations of structure and lattice dynamics of molecular crystals. *J Phys Chem A* 2012, 116:6927–6934.
125. Zheng Z-P, Fan W-H, Yan H. Terahertz absorption spectra of benzene-1,2-diol, benzene-1,3-diol and


  

benzene-1,4-diol. *Chem Phys Lett* 2012, 525–526: 140–143.

126. King MD, Buchanan WD, Korter TM. Identification and quantification of polymorphism in the pharmaceutical compound diclofenac acid by terahertz spectroscopy and solid-state density functional theory. *Anal Chem* 2011, 83:3786–3792.
127. Allen RE, De Wette FW. Calculation of dynamical surface properties of noble gas crystals. I. The quasiharmonic approximation. *Phys Rev* 1969, 179:873–886.
128. Murnaghan FD. The compressibility of media under extreme pressures. *Proc Natl Acad Sci* 1944, 30:244–247.
129. Hewat AW, Riekel C. The crystal structure of deutero ammonia between 2 and 180 K by neutron powder profile refinement. *Acta Crystallogr Sect A* 1979, 35:569–571.
130. Schatschneider B, Monaco S, Tkatchenko A, Liang J-J. Understanding the structure and electronic properties of molecular crystals under pressure: application of dispersion corrected DFT to oligoacenes. *J Phys Chem A* 2013, 117:8323–8331.
131. Manzhelii VG, Tolkachev AM, Krupskii IN, Voitovich EI, Popov VA, Koloskova LA. Thermal properties of solid $ND_3$. *J Low Temp Phys* 1972, 7:169–182.
132. Jamal M, Jalali Asadabadi S, Ahmad I, Rahnamaye Aliabad HA. Elastic constants of cubic crystals. *Comput Mater Sci* 2014, 95:592–599.
133. Rossi M, Gasparotto P, Ceriotti M. Anharmonic and quantum fluctuations in molecular crystals: a first-principles study of the stability of paracetamol. *Phys Rev Lett* 2016, 117:115702.
134. Powell BM, Dolling G, Pawley GS, Leech JW. Lattice dynamics of ammonia. *Can J Phys* 1980, 58:1703–1711.
135. Kiefte H, Breckon SW, Penney R, Clouter MJ. Elastic constants of ammonia by Brillouin spectroscopy. *J Chem Phys* 1985, 83:4738–4743.

  